POLYGONAL DELINEATION OF GREENHOUSES USING A DEEP LEARNING STRATEGY

RANJU POTE
August, 2021

SUPERVISORS:
dr. C. Persello
dr. M. N. Koeva

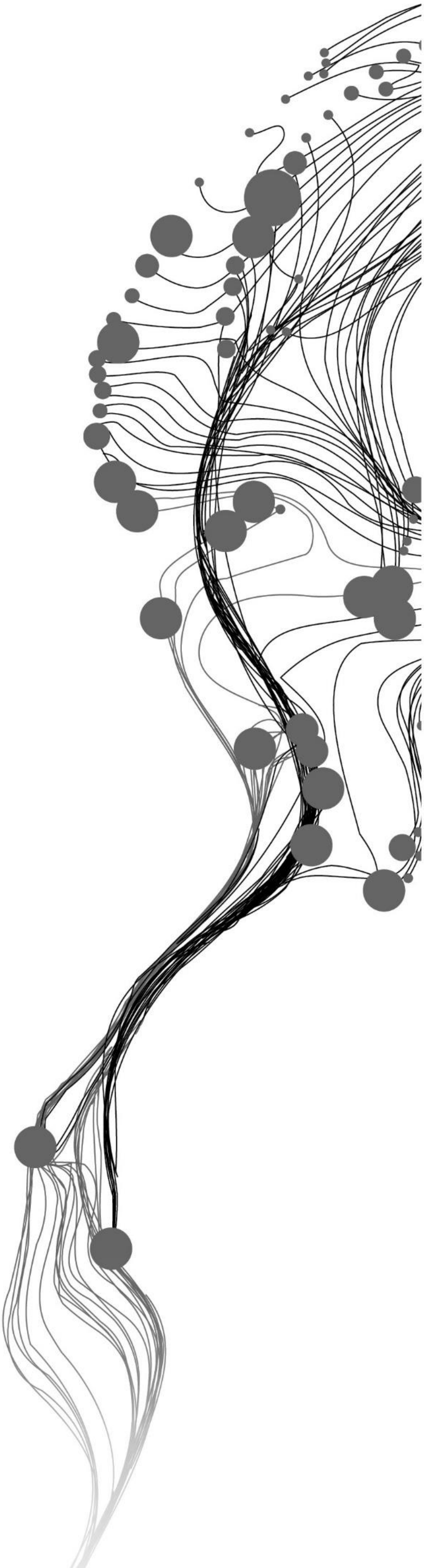

POLYGONAL DELINEATION OF GREENHOUSES USING A DEEP LEARNING STRATEGY

RANJU POTE
Enschede, The Netherlands, August, 2021

Thesis submitted to the Faculty of Geo-Information Science and Earth Observation of the University of Twente in partial fulfilment of the requirements for the degree of Master of Science in Geo-information Science and Earth Observation.
Specialization: Spatial Engineering

SUPERVISORS:
dr. C. Persello
dr. M. N. Koeva

THESIS ASSESSMENT BOARD:
Prof.dr.ir. A. Stein (Chair)
dr. Dalton D Lunga (External Examiner, Oak Ridge National Laboratory, USA)

ABSTRACT

Geoinformation update and maintenance are crucial for planning, decision-making processes and geospatial analysis. In the Netherlands, the Dutch cadaster (Kadaster) handles the geodata maintenance, and updates those datasets. As per the Dutch Kadaster, "The digital map is still being built". 'Basisregistratie Topografie' (BRT) registry of the Kadaster contains the geospatial information of objects such as buildings, the agricultural field, roads, and tracks, which are freely available as open data. One of the objects of interest is the greenhouses used for horticulture purposes. The greenhouses are being manually delineated for updating the geodata set. Kadaster has been using deep learning approaches for object recognition. However, state of the art image segmentation models applied in Kadaster typically output segmentation in raster format. The applications of geographic information systems often require vector output. Additionally, there is a considerable research gap for the delineation of greenhouses through the deep learning (DL) method in vector format. Thus, this study aims at developing a DL technique to extract the greenhouses in a vector format.

There are two state of the art methods for vectorization using deep building segmentation. First is an end-to-end method that learns the vector representation directly, and secondly, vectorizing the classification map by a network. In this study, the second state of the art method was utilized. Girard et al. (2020) introduced a building delineation method based on frame field learning to extract the regular building footprints in polygonal vector format using aerial RGB imagery. The method was utilized in the greenhouse, where a fully convolution network (FCN) was trained to simultaneously learn the mask of the greenhouse, contours and the frame field, followed by polygonization. The contours information in the frame field produces regular outlines which accurately detects the edges and the corners of the greenhouse.

The study was conducted within the three provinces of the Netherlands. Two orthoimage datasets of summer and winter images with the resolution of 0.25 m and 0.1 m, respectively, were used. The normalized digital surface model (nDSM) was added to the winter RGB images to extract the accurate and regular greenhouse polygons. The addition of nDSM improved the prediction and outlines of the greenhouses compared to using only 0.1 m winter RGB images. The mean intersection over union (IoU) of (RGB + nDSM) for 0.1m images was 0.751, while for the same resolution dataset, the IoU was 0.673, indicating the improvement of greenhouse delineation accuracy with the addition of height information. The IoU for 0.25m RGB image was 0.745 and could predict the greenhouses, which 0.1m RGB image could not. The qualitative analysis of the result shows the regular and precise predicted polygons.

ACKNOWLEDGEMENTS

Firstly, I would like to express my sincere gratitude to my supervisors: dr. Claudio Persello and dr. Mila Koeva from ITC and Diede Nijmeijer and Marieke Kuijer from the Kadaster for their continued guidance, support and valuable discussions, which enabled me to complete my thesis. I want to express my sincere thanks to Kadaster for giving me the opportunity to conduct the research and do my internship in their organization. I also want to thank Wufan Zhao for his help during the initial phase of the research.

I extend my thanks and appreciation to the Geo Expertise Center department, object recognition team for their constructive feedback and valuable guidance during the research phase in the internship. I want to extend heartly thank the manager Stefan Besten of the Kadaster for extending my internship time period for further experimental analysis on the research.

Most importantly, my sincere thanks to my family and friends for their love, advice, encouragement and their constant support when I was struggling. Without them, it would have been a difficult journey.

TABLE OF CONTENTS

LIST OF FIGURES

LIST OF TABLES

LIST OF ABBREVIATIONS

AP	Average Precision
AR	Average Recall
BCE	Binary-cross entropy
BGT	'Basisregistratie Grootschalige Topografie' Or Basic Registration Large-Scale Topography
BRT	'Basisregistratie Topografie'
BZK	Minister of the Interior and Kingdom Relations
CIR	Color InfraRed
CNN	Convolutional Neural Network
COCO	Common Objects in COntext
DL	Deep Learning
DSM	Digital Surface Model
DTM	Digital Terrain Model
FCN	Fully Convolutional Network
GeoJSON	Geospatial Javascript Object Notation
GPUs	Graphics Processing Units
LULC	Land Use and Land Cover
LIDAR	Light Detection and Ranging
MLC	Maximum Likelihood Classification
nDSM	Normalized Digital Surface Model
PDOK	Publieke Dienstverlening Op de Kaart or Public Services On the Map
R-CNN	Region-based Convolutional Neural Networks
ROI	Region of Interest
VHR	Very High-Resolution
WLD	ESRI World
WV	WorldView

1. INTRODUCTION

1.1. Background

Earth observation has largely broadened the range of applications with the availability of very high-resolution (VHR) overhead images captured from airborne or satellite platforms (Kaiser et al., 2017). There is a vast amount of data available with different spatial, spectral and temporal resolutions. In the Netherlands, an abundance of geodata is available with VHR aerial imagery and light detection and ranging (LIDAR) data with the height model, which are freely available to the public (Kadaster, n.d.-c). With the vast amount of data, and inevitable changes occurring in the area (Cheng et al., 2017), there is a need to keep an updated geo-information database within the nation. The updated information can be used for planning, decision-making processes and geospatial analysis.

VHR imagery has been used for object detection and extraction with high accuracy and reliable information (Chen et al., 2019; Shrestha & Vanneschi, 2018; Tayara & Chong, 2018). The high intra-class spectral variability among the same objects makes it difficult to solve the classical pixel-based classification problem (Girshick et al., 2014). According to Carrilho and Galo (2019), with high-resolution aerial imagery, complexity increases, which requires robust pattern recognition networks. Deep learning (DL) is a subset of machine learning, in which the algorithm learns the patterns through labelled training data (Hoeser & Kuenzer, 2020). Krizhevsky, Sutskever, and Hinton (2012) introduced convolutional neural networks (CNNs), which made DL popular in the computer vision society for image recognition of natural images. According to Hoeser and Kuenzer (2020), DL concepts from computer vision are transferred to earth observation applications for overhead images. The same authors also mentioned that DL methods have become popular with large data availability and faster processing units such as Graphics Processing Units (GPUs). Potlapally et al. (2019) mentioned that DL is used for extracting the high-level features from the input images. DL has been a growing field for the application on Earth observation such as land use and land cover (LULC) classification (Potlapally et al., 2019), building footprints (K. Zhao et al., 2020), road network (Buslaev et al., 2018), and vehicle detection (Gandhi, 2018).

DL is also reliable for automatically extracting objects of interest such as buildings and roads using aerial or satellite images (Montoya-Zegarra et al., 2015; Pan et al., 2019; Saito & Aoki, 2015; Shrestha & Vanneschi, 2018). Usually, the VHR images captured from aerial platforms have a low spectral resolution. Still, they have a very high spatial resolution, so they are mainly used for segmentation or detection rather than classification or recognition (Hoeser & Kuenzer, 2020). Image recognition means predicting the class label for a whole image, and traditional CNN solves the classification problem. Figure 1 shows the visual difference between these terms on computer vision. The fundamental step of automatic mapping is semantic segmentation. Each pixel is labelled with the class, i.e., the prediction is made for every pixel. Fully convolutional networks (FCNs) are considered the state-of-the-art for semantic segmentation (Long et al., 2015).

In object detection, the location of one or more objects in the image is identified, and bounding boxes are drawn around their extent with classes of the located objects (Brownlee, 2019; Su et al., 2019). Figure 1-c shows the detected object of interest and bounding box surrounding it. For object detection, Faster Region-based Convolutional Neural Networks (Faster R-CNN) utilizes a network to predict the region proposals which are reshaped using a Region of Interest (ROI) pooling layer, which later is utilized to classify the image within the proposed region to predict the offset values for the bounding boxes. Instance segmentation can be modelled as a multi-task problem where objects are precisely determined and segmented in each instance (P. L. Liu, 2020). It uses both the elements of object detection and semantic segmentation. The objects of interest are classified at an individual level with localization within a bounding box, and each pixel is classified within certain categories (He et al., 2020; Liu et al., 2018). Mask R-CNN architecture is a state-of-the-art model for instance segmentation, which is built with Faster R-CNN; in which the object of interests are represented within the bounding boxes and the additional branch predicts the object mask (He et al., 2020). It means that it parallelly predicts the masks and the class labels of the object of interest in the image. Mask R-CNN is applied with an instance-first strategy in which the first object of interest is determined with the bounding box, and inside the bounding box, per-pixel classification is done with the output as the masked object with the bounding-box and class label in it (He et al., 2020; Su et al., 2019).

a. Aerial Image

b. Semantic Segmentation

c. Object Detection

d. Instance Segmentation

Figure 1: Computer vision tasks where the orange part denotes the greenhouse
Adapted from : (Hoeser & Kuenzer, 2020)

Nonetheless, for many geographic information systems applications, assigning a label to each pixel describing the category is not the final desired output. Image segmentation is an intermediate step if the objective of the work is to do object shape refinement, vectorization, and map generalization. Thus, there is a necessity to modify the conventional raster-based pipeline. Li, Wegner, and Lucchi (2019) developed a learnable framework, called PolyMapper which can predict the outline of the buildings and roads in a vector format from the aerial images directly. The approach directly learns the mapping with a single network architecture, which used to be a multi-step procedure of semantic segmentation followed by shape improvement with converting the building footprints and roads to polygons and refining those polygons. W. Zhao et al. (2021) modified the baseline method of the PolyMapper and established a new model with an end-to-end learnable model. It extracts the outline of polygons from VHR imagery, which can segment building instances of various shapes with greater accuracy and regularity. Girard, Smirnov, Solomon, and Tarabalka (2020) proposed a framework based on a deep image segmentation model using remote sensing images for building polygon extraction. It utilizes FCN for pixel-wise classification and add frame field to it obtain the building's vectorized polygonization. The segmentation is improved via multi-task learning with the addition of frame field aligned to object tangents.

This research will focus on the delineation of greenhouses in the Netherlands. Greenhouses are built for agriculture and horticulture purposes. The detection, monitoring, and mapping of the greenhouses are essential for urban and rural planning, crop planning, sustainable development, risk on the rapid expansion of the greenhouses, for example, accumulation of vegetable and plastic waste, over-exploitation of water greenhouse, natural encroachment causing harm to the environment (Aguilar, Saldaña, & Aguilar, 2013; Celik & Koc-San, 2018, 2019; Dilek Koc-San, 2013). According to several authors (F. Agüera et al., 2006; Carvajal et al., 2010; Celik & Koc-San, 2018; D. Koc-San & Sonmez, 2016; Novelli et al., 2016), greenhouse delineation and mapping is a challenging task due to the changing spectral reflectance value obtained back in the sensor and due to the crops beneath the greenhouse. There are different classifications of greenhouses, such as a plastic-covered, glasses-covered, plain sheet, and corrugated sheet (fibre-glass reinforced plastic) greenhouse (Tiwari, n.d.). The spectral signature from different types of the greenhouse also changes drastically, making it difficult to automatically detect and classify the greenhouses (Agüera et al., 2008a). The state-of-art in the study of the greenhouse is only limited to object classification. The novelty of the study is that there is no study done based on the DL techniques for the automatic greenhouse extraction in regularized vector format.

1.2. Problem statement

According to the Dutch Kadaster, "The digital map is still being built" (Kadaster, n.d.-d). Greenhouses are part of the 'Basisregistratie Topografie' (BRT) (further described in section 2.1.1.2.) in TOP10NL as the objects. In Kadaster, greenhouses are being manually digitized. There is still a need for methods to extract, label, and update the greenhouse for the countries' geodatabase. The governmental organization, private companies, and the public can utilize the updated geodata information properly. One of this study's motivations is the project required by Kadaster on updating BRT in terms of the greenhouses. Furthermore, there is a considerable research gap between the highly researched automatic building detection and delineation through deep learning for VHR aerial images and automatic greenhouse delineation through deep learning methods. Instance segmentation and polygonal mapping of the greenhouses is the major innovative point of the research, as there is no study related to automatic extraction through instance segmentation or object detection using DL in the case of the greenhouse.

1.3. Geodata updating as a wicked problem

Geo-information data needs to be revised regularly such that all the users of the data can utilized the updated data for analysis of a spatial problem. The updated information plays a role in spatial planning and governance, making it a wicked problem. So, there is a need of up to date geodata in an efficient way. Manual delineation of the data for updating geoinformation is time-consuming and expensive. Automation is necessary as it helps to save time and be more efficient with the use the resources. So, a way to minimize the process of updating geodata can help in lessening the wicked problem.

1.4. Research objective

1.4.1. General objective

This thesis's general objective is to develop a deep learning approach for greenhouses detection and delineation in polygon format using VHR aerial imagery and elevation data for the geodata update.

1.4.2. Specific objective

The main research objectives can be achieved through the following specific sub-objectives and research questions (RQs):

1. To develop a method to perform instance segmentation of the greenhouses, more specifically, a DL technique that can extract object instances in a vector format (polygon).

RQ1: Which deep learning or CNN architecture is appropriate for automated delineation of greenhouses in the polygon format?
RQ2: Which cadastral data sets are suitable for the experimental analysis?
RQ3: Does the normalized Digital Surface Model (nDSM) data contribute to more accurate detection and segmentation of greenhouses?
RQ4: What is the effectiveness of the approach for different types of greenhouses (plastics and glasses)?

2. To compare different datasets combination to determine for greenhouse delineation

RQ5: Which dataset performs better in terms of delineation of greenhouses?
RQ6: What is the accuracy of the polygonized greenhouse with the standard metrics?

3. To update the greenhouse polygons in the cadastral database.

RQ7: What are the specification required by Kadaster to update the BRT in terms of the greenhouse?
RQ8: How can the above technique be used for regular updating of the cadastral database of greenhouses?

1.5. Thesis Structure

This thesis contains seven chapters organized as follows:

a. Chapter 1 presents the introduction that explains the background and the problem statement, research objectives, and research questions that the thesis wants to answer.
b. Chapter 2 provides the conceptual framework, stakeholders involved, and the literature reviews to support the research
c. Chapter 3 explains in detail the research methodology used in this thesis.
d. Chapter 4 includes the materials used in the thesis, describing the study area, data used and pre-processing of those data.
e. Chapter 5 describes the experimental analysis and description of the evaluation metrics that are used in the thesis.
f. Chapter 6 shows the result and discussion of the experimental analysis.
g. Chapter 7 contains the conclusion, answer to the research questions and recommendation.

2. CONCEPTUAL FRAMEWORK AND RELATED WORKS

This chapter describes the conceptual framework, describing the systems and subsystems involved in the study. Additionally, the literature's related works on mapping the greenhouses and existing deep learning methods are discussed.

2.1. Conceptual Framework

Figure 2 shows the main conceptual framework of the study. The TOP10NL BRT product for greenhouses needs to be regularly updated as there are changes in the greenhouses' numbers, location, and size. Currently, in the Dutch cadaster (Kadaster), manual digitization is used for updating the datasets. In this study, deep learning concepts are introduced; so that automation helps speed up the manual updating process for delineation of the greenhouse. If the vectorized greenhouse satisfies the specification of the BRT, then it can be used for updating it.

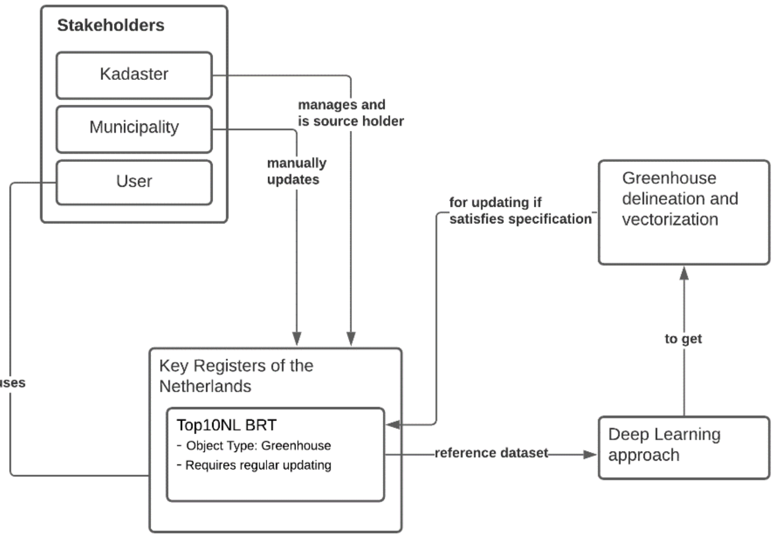

Figure 2: Conceptual framework for delineating greenhouse with the involvements of stakeholders

2.1.1. Key Registry of the Netherlands

The basic registration is an officially designated registration by the government, which contains high-quality data, which needs to be used mandatory by all government agencies and is the product that can be used without further investigation (Kadaster, 2020). Topographical key registrations contain spatial information and are therefore very useful for solving geo-related tasks. The main purpose of a topographical key registration is to reuse the dataset many times as a base for many geo-related tasks. In the Netherlands, there are many different 'Registraties' i.e. Registrations within the Land Registry of the Key Registers and National Facilities (Ministerie Van Binnenlandse Zaken en Koninkrijksrelaties, n.d.). Only the overview of 'Basisregistratie Grootschalige Topografie' (BGT) and 'Basisregistratie Topografie' (BRT) will be outlined in this study as they are the most relevant topographical key registrations in terms of greenhouses.

2.1.1.1. 'Basisregistratie Grootschalige Topografie' (BGT)

BGT is a division of topographical key registrations with a detailed digital map of the Netherlands with an accuracy of up to 20cm (Digitale-overheid.nl, n.d.). It is used as the base map of the Netherlands with the location of the objects, for instance, buildings, roads, water, railway lines and greenery (agricultural sites) on a larger scale, which is registered unambiguously (Information about the Register of Large-Scale Topography (BGT) - Land Registry Business, n.d.). BGT is object-oriented topographical key registration for large scales from 1:5,00 to 1:5,000. Kadaster manages BGT with 392 source holders such as municipalities, provinces and water boards with the BZK, the Ministry of Defense, Rijkswaterstaat and ProRail, who works on their part for the completeness and uniformity of the BGT (Kadaster, n.d.-c). The BGT geodata is essential for planning green management, presenting plans for urban renewal, planning evacuation routes, so updating the geodata is essential (Ministerie van Binnenlandse Zaken en Koninkrijksrelaties, n.d.-a).

2.1.1.2. 'Basisregistratie Topografie' (BRT)

BRT contains both the objects and the raster digital topographic files (TOPNL and TOPraster data) with different scales for the whole of the Netherlands. The data available is in the map format and the object-oriented files that are freely available as open data (Key Register Topography (BRT), n.d.). Top10NL is a digital topographic file within a scale ranging from 1:5,000 to 1:25,000. TOP10NL is suitable for geometric reference and used as a basis for GIS and web applications. It is also a standard for analogue topographic maps with the scales of 1:10,000 and 1:25,000. From 2013, the digital file of scale 1:50,000 is being produced by automatic generalization. TOP10NL is the standard basic topographic file for use within the government in the relevant scale area (Kadaster, 2020). It contains the information of the greenhouses in the digital format regarding the type of greenhouses and area occupied.

2.1.2. Stakeholders

Stakeholders are the individuals or organizations who have interest, power or influence in a decision (Hemmati, 2002). The identified stakeholders are described below:

2.1.2.1. Dutch Kadaster

Kadaster is the non-departmental public body in the Netherlands, which is the country's Cadastre, Land Registry and Mapping Agency. It operates under the political responsibility of the Minister of the Interior and Kingdom Relations (BZK). It is involved in collecting, registering administrative and spatial data on the property. It is also responsible for national mapping along with the maintenance of the national reference coordinate system of the Netherlands. It is also the advisory body for land-use issues and national spatial data infrastructures (Kadaster, n.d.-a). If the Dutch governments such as ministries, provinces, municipalities and other governmental services need to work with the maps, they must use the geodatabase provided by Kadaster.

2.1.2.2. Municipalities

Municipalities are the small bodies of the government that are responsible for carrying out the tasks that directly affect the residents. There are 358 municipalities in the Netherlands, and each municipality has to work on the data of their location (Government.nl, n.d.).

2.1.2.3. Users

The users are the public, governmental bodies, and greenhouse owners who use the data and services to view the information or utilize the data for analysis.

2.1.3. Stakeholder Analysis

A stakeholder analysis was conducted to see the power and interest of the relevant stakeholders from the conceptual diagram, as shown in figure 2. A literature review was conducted regarding the interest of the stakeholder.

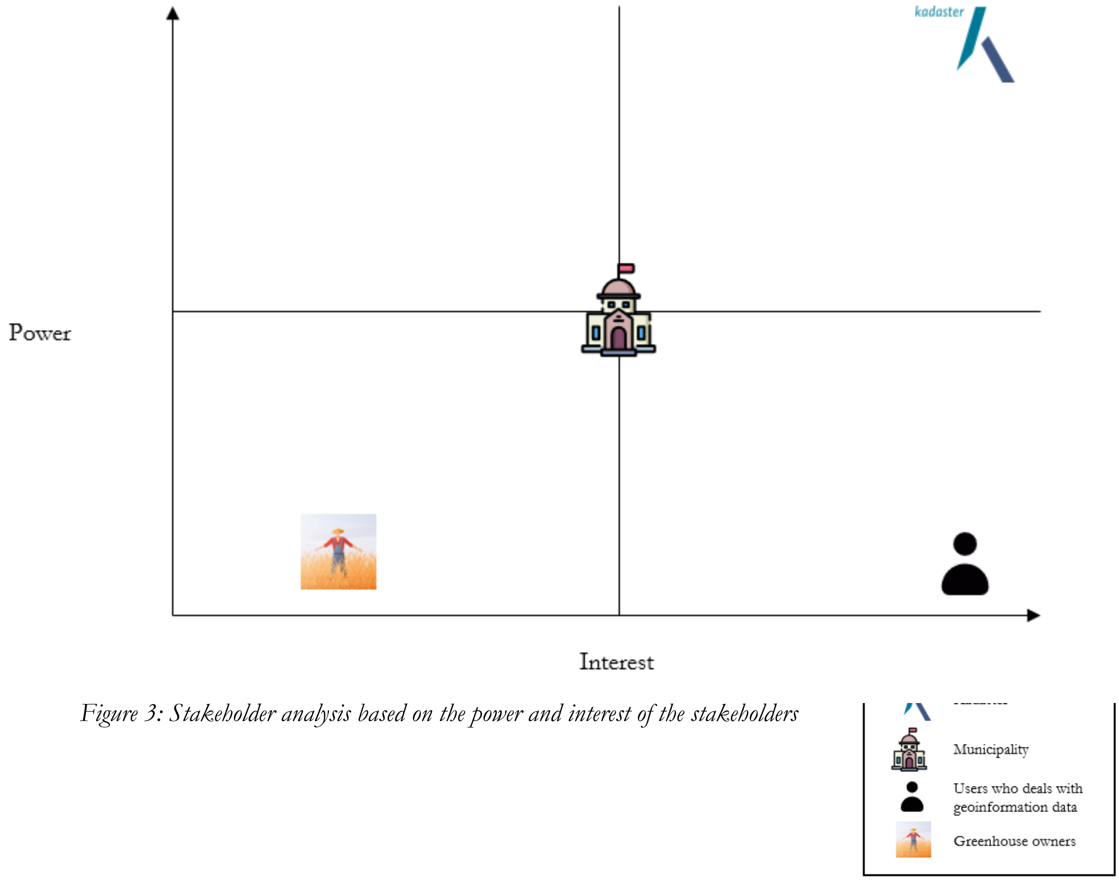

Figure 3: Stakeholder analysis based on the power and interest of the stakeholders

The power and interest of the stakeholder in terms of the requirement of up to date geodata information and the methodology to delineate the greenhouse is shown in figure 3. Kadaster has high interest and high power to update the geoinformation in terms of greenhouse and to develop a methodology to delineate the greenhouse as they have been updating the digital information data of the Netherlands (Digitale-overheid.nl, n.d.). The municipality manages the geoinformation within their location, which requires the up to date geoinformation as all the government institutions are required to use the geodata information for public-law tasks involving geodata information (Ministerie Van Binnenlandse Zaken en Koninkrijksrelaties, n.d.). However, Kadaster manages the BRT dataset, so the municipality does not have a role in the BRT dataset in terms of methodology needed to be delineated. The users who deal with the geoinformation data are interested in up to date information to do their analysis. The users are more interested in the dataset within certain standards than how they were obtained. Their interest mainly lies in the end product, so they do not have a role in the methodology being developed to delineate the greenhouse. The greenhouse owners have the least power and interest in terms of methodology to be developed for delineation of greenhouses, as they can view the data of the greenhouse in the geodatabase.

Figure 3 shows that Kadaster is the main stakeholder with the most power and interest. The thesis mainly focuses on the methodology to delineate the greenhouses; the needs and requirements of the Kadaster are taken into account. The specifications or the criteria that define a greenhouse was questioned to Kadaster, which involved handling the digital objects to be included in the BRT. D.Nijmeijer (personal communication, July 13, 2021) pointed out the specifications required by Kadaster to update the BRT in terms of the greenhouses as:

- Greenhouses should be bigger than 200 sqm, and greenhouses less than 200sqm is not considered greenhouse,
- Greenhouses with plastic are only considered to be a greenhouse if they are permanent in nature. Otherwise, greenhouses made up of glasses are only considered to be defined as greenhouse,
- If the greenhouse is moveable, it is not necessary to detect the new position.

2.2. Literature Review

This section is divided into two parts: one for the study review on greenhouses and the other for the instance segmentation and the polygonization done on the buildings. Greenhouse usually has similar structures with simple buildings. There is no research on automatic extraction and delineation of greenhouses in vector format using the deep learning method, the existing literature on deep building segmentation is considered. The literature on extraction on the building is shown in Table 1, which describes the summary of related studies on the greenhouses with remote sensing datasets, the method applied and the results.

Table 1: Related studies on greenhouses classification

Study No	Title	Remote Sensing Datasets	Method	Results	Reference
1	"Detecting greenhouse changes from QuickBird imagery on the Mediterranean coast"	QuickBird multispectral imagery	It is based on the maximum likelihood classification method with different band combinations for classification and comparing the current image with the information system.	The band combination of G-B-NIR obtained the quality percentage (QP)of 87.11% and greenhouse detection percentage, i.e., recall of 91.45%	(F. Agüera et al., 2006)
2	Using texture analysis to improve the per-pixel classification of VHR images for mapping plastic greenhouses	QuickBird and IKONOS satellite image	Maximum Likelihood Classification (MLC) with a different combination of bands of R, G, B, NIR, and panchromatic bands	QuickBird image had a better result than IKONOS images, and the inclusion of texture information in classification did not improve the classification quality of plastic greenhouse	(Agüera et al., 2008b)
3	"Mapping Rural Areas with Widespread Plastic Covered Vineyards Using True Color Aerial Data"	Digital true colour aerial data captured using an Intergraph's Z/I	Image segmentation followed by classification based on eCognition software provides a data mining functionality called Feature Space	Segmentation followed by the object-oriented approach is better for mapping plastic-covered vineyards showing an overall	(Tarantino & Figorito, 2012)

Study No	Title	Remote Sensing Datasets	Method	Results	Reference
		Imaging Digital Mapping Camera (DMC)	Optimization (FSO); to calculate features in OBIA context, i.e. like spectral (image bands, band ratios), geometrical (area, compactness), contextual (difference to a neighbour), and textural properties.	accuracy of 90.25% for all the classes in the classification.	
4	"GeoEye-1 and WorldView-2 pan-sharpened imagery for object-based classification in urban environments"	Pan-sharpened orthoimages from both GeoEye-1 and WorldView-2 (WV2) VHR satellites	OBIA software, eCognition v. 8.0, was used to segment the image with the multi-segmentation method. The features used for classification considered spectral, geometry, texture, and elevation features. Then the authors opted for manually classifying the segments to their respective classes.	The accuracy for the GeoEye-1 image was close to 89% when spectral and elevation was taken into consideration. WV2 obtained 83% accuracy with the same feature. No improvement on classification was seen with the new spectral bands of WV2 (Coastal, Yellow, Red Edge, and Near Infrared-2).	(Aguilar et al., 2013b)
5	"Evaluation of different classification techniques for the detection of glass and plastic greenhouses from WorldView-2 satellite imagery"	WorldView-2 satellite imagery	For land cover classification; Maximum likelihood (ML), random forest (RF), and support vector machines (SVM) are used as a classifier with emphasis on greenhouse detection.	ML had higher accuracies compared to SVM and RF classifiers.	(Dilek Koc-San, 2013b)
6	"Methodological proposal to assess plastic greenhouses land cover change from the combination of archival aerial orthoimages and Landsat data"	Archival aerial orthoimages (produced by the Spanish or Andalusia Governments)	Object-based greenhouse mapping was done by using image segmentation in eCognition v. 8.8 software using bottom-up region-merging technique and multi-resolution segmentation algorithm. It was	The OA on combined orthoimage and LandSAT was higher than the OA on individual datasets.	(González-Yebra et al., 2018)

Study No	Title	Remote Sensing Datasets	Method	Results	Reference
		and Landsat imagery	followed by OBIA classification with features such as mean values, standard deviation, shape index and brightness were used in the same software.		
7	"Greenhouse Detection Using Aerial Orthophoto and Digital Surface Model"	Digital aerial photos and digital surface model (DSM)	For greenhouse detection, Support Vector Machine (SVM) classifier was used to classify the orthophoto and nDSM was used as the additional data	Producer accuracy (PA) for greenhouse classification is 94.50%, and user accuracy (UA) is 95.80%.	(Celik & Koc-San, 2018)
8	"Greenhouse Mapping using Object-Based Classification and Sentinel-2 Satellite Imagery"	Sentinel-2 Multispectral Instrument (MSI) data	Object-based classification with multi-resolution segmentation was used. Spectral features like mean values, Normalized difference vegetation index (NDVI), Normalized difference water index (NDWI) were extracted for OBIA classification by applying the nearest neighbour classifier.	The average user accuracy for the greenhouse class was 96%, and PA for the greenhouse was 80%.	(Balcik et al., 2019)
9	"Greenhouse Detection from Color Infrared Aerial Image and Digital Surface Model"	Colour and infrared orthophotos, normalized Digital Surface Model (nDSM),	OBIA was used to calculate the Normalized Difference Vegetation Index (NDVI) and Visible Red-based Built-up Index (VrNIR_BI). Multi-Resolution Segmentation method was used for segmentation and for classification, K-Nearest Neighbor (K-NN), Random Forest (RF) and Support	The literature suggests that only 2D information is not sufficient for greenhouse detection, and utilizing both 2D and 3D information from the colour orthophoto with the nDSM using OBIA detects the greenhouse effectively. The SVM classifier had a high PA of 96.88% and	(Celik & Koc-San, 2019b)

Study No	Title	Remote Sensing Datasets	Method	Results	Reference
			Vector Machine (SVM) techniques were used.	UA of 98.10% among the classifier.	
10	"Mapping Plastic Greenhouses Using Spectral Metrics Derived From GaoFen-2 Satellite Data"	VHR optical satellite data (GaoFen-2 image)	First, the calculation of spectral characteristic analysis for land covers was done. A three-step procedure for classification was done where the index was used for classification. Double Coefficient Vegetation Sieving Index" (DCVSI), "High-Density Vegetation Inhibition Index" (HDVII) and Normalized Difference Vegetation Index (NDVI) were used.	DCVSI enhanced the vegetation information and explicitly distinguished between greenhouse and vegetation on another land surface. HDVII was used to eliminate high-density vegetation explicitly, and NDVI to distinguish the plastic greenhouse.	(Shi et al., 2020)

Table 2 summarises related studies on the instance segmentation with remote sensing datasets, methods used, and the results, particularly for the buildings instances. There are no particular studies done on a greenhouse on the relative method.

Table 2: Related studies on instance segmentation on buildings

Study No	Title	Remote Sensing Datasets	Method	Results	Reference
1	"Mask R-CNN"	Natural images	Mask R-CNN is state of the art; in instance segmentation, a branch for object mask prediction in parallel to the existing branch of bounding box recognition is used.	In COCO suite challenges, for instance segmentation, person keypoint detection and bounding box object detection, it outperformed the COCO 2016 winner.	(He et al., 2020)
2	"Instance Segmentation in Remote Sensing Imagery using Deep	High resolution orthogonal aerial images obtained from earth explorer	Mask R-CNN is used where proposals are generated in the images classifies the	For the detection of objects of interest, the mean average precision (mAP) at the IoU	(Potlapally et al., 2019)

Study No	Title	Remote Sensing Datasets	Method	Results	Reference
	Convolutional Neural Networks”		ROI for segmentation mask and bounding box along with the object of interest such as tress, crop fields, cultivated lands and water bodies.	threshold of 0.5 was 0.527.	
3	“Automatic Object Extraction from High-Resolution Aerial Imagery with Simple Linear Iterative Clustering and Convolutional Neural Networks”	High-resolution aerial images	The method uses object extraction similar to Fast R-CNN architecture and uses a simple linear iterative clustering (SLIC) algorithm for ROI generation.	Multi-scale SLIC generates ROI of different sizes and objects detection and segmentation with an overall accuracy (OA) of 89%.	(Carrilho & Galo, 2019)
4	“Boundary Regularized Building Footprint Extraction from Satellite Images using Deep Neural Networks”	High-resolution satellite images of DigitalGlobe Worldview-3 Satellite	The method, namely R-PolyGCN, is a two-stage object detection network to produce ROI features and use graph models to learn geometric information for building boundary extraction.	The F1 score is 0.742 for building extraction, and for building regularization, R-PolyGCN predicts the natural representation for the vertex, edges and the polygon.	(K. Zhao et al., 2020)
5	“Object Detection and Instance Segmentation in Remote Sensing Imagery Based on Precise Mask R-CNN”	VHR remote sensing images acquired from Google Earth	The framework is based on Mask R-CNN, including RPN and Fast R-CNN classifier with Precise RoI pooling instead of RoI align.	For object detection, AP is 61.2, and for segmentation performance, AP is 64.8.	(Su et al., 2019)
6	“TernausNetV2: Fully convolutional network, for	High-resolution satellite imagery	FCN network called TerausNetV2 uses encoder-decoder type architecture with skip	For DeepGlobe-CVPR 2018, building detection sub-challenge, based on public	(Iglovikov et al., 2018)

Study No	Title	Remote Sensing Datasets	Method	Results	Reference
	Instance segmentation”		connection with the encoder called ABN WideResNet-38 network and in-place activated batch normalization.	leaderboard score, the model scored 0.74	
7	“Building Instance Change Detection from Large-Scale Aerial Images using Convolutional Neural Networks and Simulated Samples”	VHR aerial images	The framework consists of building an extraction network using Mask R-CNN for object-based instance segmentation and FCN for pixel-based semantic segmentation to build a binary building map.	Both object-based and pixel-based model’s evaluation measured are used. Without using a real change sample, the AP of building instance was 0.63, Precision of 0.64 and Recall of 0.943.	(Ji et al., 2019)
8	“Topological Map Extraction from Overhead Images”	VHR aerial images	Method named Polymapper for pixel-wise segmentation for directly predicting the polygons of the buildings and the roads. It uses CNN as the backbone for feature learning and integrates with the feature pyramid network for bounding boxes for buildings. It uses a skip feature map with the bounding box obtained and RNN to get the vertices of the polygons of the buildings.	Evaluated with the standard MS COCO measures with AP of 55.7 and AR of 62.1. In which AP and AR for small buildings were lower compared to medium and large buildings.	(Z. Li et al., 2019)
9	“Building Outline Delineation: From Very High-Resolution	VHR aerial images	Modified the baseline method of the PolyMapper by using EffcientNet	For COCO metrics on the building delineation, the applied method had	(W. Zhao et al., 2020)

Study No	Title	Remote Sensing Datasets	Method	Results	Reference
	Remote Sensing Imagery to Polygons with an Improved end-to-end Learning Framework”		as backbone feature encoder to the network and for better prediction accuracy of the corner, using the Boundary Refinement block (BRB).	an AP value of 0.445. The average Recall value of 0.499. It can correctly segment the building instances of various shapes and sizes with more compact and regularized shapes.	
10	“Polygonal Building Segmentation by Frame Field Learning”	VHR aerial images	Method named Frame Field Learning for pixel-wise segmentation and addition of frame field as output for polygonization of the buildings.	The method is useful for the regularization of the sharp corners of the building and can handle holes in the buildings and walls in the adjoining building.	(Girard et al., 2020)

Table 3 describes the summary of related studies on the vectorization for deep building segmentation, which is divided into two different categories with remote sensing datasets, methods used, description about the method and the problems within the method for the buildings instances as there are no particular studies done on a greenhouse on the comparative method.

Table 3: A related study on vectorization for deep building segmentation

S.No	Category	Method used	Problems encountered
1.	Classification map produced from deep learning network and vectorizing the classified map	Contour detection (marching squares method (Lorensen & Cline, 1987)) for constructing 3D surfaces by forming triangle modes of constant density surfaces and followed by polygon simplification (Ramer, 1972) algorithm where small-but not minimum-number of vertices within the curve is utilized to form a polygon.	Sharp corners are not produced when the classification map is not perfect when the conventional deep segmentation method is used. The expensive and complex post-processing procedure required to improve final polygons
		In the classification map, the approximate shape of the object is done using the polygonal partition refinement method(M. Li et al., 2020), where progressively extended detected line segments are added together to form polygons. The	The tuneable parameter does not control the exact number of output vertices compared to the other vectorization pipelines.

S.No	Category	Method used	Problems encountered
		trade-off between complexity and fidelity is done using a tuneable parameter.	
		FCN with a shared decoder and discriminator was used to train with the combination of adversarial and regularized losses to produce cleaner building footprints (Zorzi & Fraundorfer, 2020).	The method is less stable than conventional supervised learning as it requires the computation of large matrices of pairwise discontinuity costs between pixels and the adversarial training system of networks.
2.	Deep learning segmentation method to directly learn vector representation (end-to-end method)	Curve-GCN method: The prediction of all vertices simultaneously using graph convolutional network (GCN) is trained to deform a polygon to fit each object (Ling et al., 2019).	GCN is difficult to train compared to CNN and is only suitable for simple polygons without holes.
		Polymapper method: It localizes the object of interest with a combination of the Feature Pyramid Network (FPN) for localization of the object of interest, detection of Region of Interest (ROI) in the image and PolygonRNN for the geometrical shape of the single (individual) object (Z. Li et al., 2019).	It is not suitable for complex buildings, and although adjacent buildings are detected as individual polygons, the shared edges within the buildings are not aligned.

3. RESEARCH METHODOLOGY

The existing work for vectorization using deep building segmentation have two categories, i.e., an end-to-end method that learns the vector representation directly, and the other is vectorizing the classification map by a network. For delineation of greenhouses using deep learning methodology, both categories were investigated in this study.

3.1. Method I: Polymapper

The polymapper method is the end-to-end learning method that directly extracts the object of interest's polygon shape (mainly buildings and roads) with the provided aerial image and reference data. The method is used to achieve instance segmentation of the geometrical shapes of the buildings in the aerial images. Polymapper would help to detect (localize) all the objects of interest and precisely segment each object of interest in the polygon representation rather than a per-pixel mask. Polymapper is the combination of the Feature Pyramid Network (FPN) for localization of the object of interest, detection of Region of Interest (ROI) in the image, and PolygonRNN for the geometrical shape of the single (individual) object (Z. Li et al., 2019; W. Zhao et al., 2020).

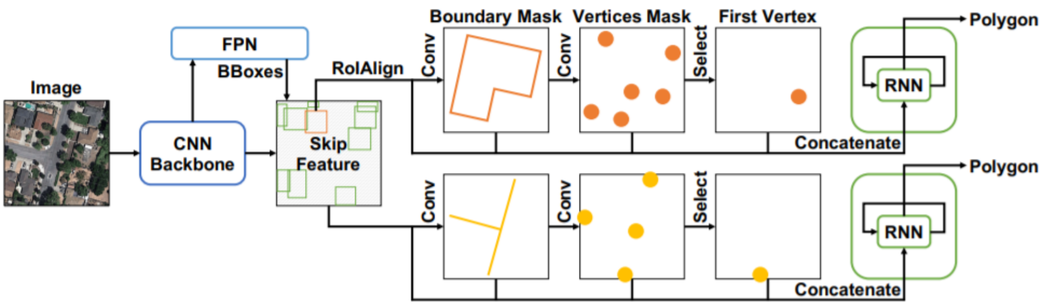

Figure 4: Workflow of investigated polymapper method for buildings using RGB images and reference data

Adapted from : (Li, Wegner, & Lucchi, 2019)

3.2. Method II: Frame field learning

Girard, Smirnov, Solomon, and Tarabalka (2020) proposed a framework based on a deep image segmentation model using remote sensing images for buildings. It utilizes FCN for pixel-wise classification and adds frame fields to obtain buildings' vectorized polygonization. Girard et al. (2020) has defined frame field as a 4-PolyVector field which is locally defined by two symmetric line fields, called frames. The frame is defined by two directions at each point in the image as two complex numbers $u, v \in \mathbb{C}$. The coefficients are represented as the complex polynomial in which the two directions are converted into coded form with relabelling and change of sign:

$$f(z) = (z^2 - u^2)(z^2 - v^2) = z^4 + c_2 z^2 + c_0 \tag{1}$$

Within the set of pairs of directions, the constants $c_0, c_2 \in C$ uniquely determines an equivalence class corresponding to a frame. The equation (1) can be denoted as $f(z;\ c_0, c_2)$. One of the pair of directions, (c_0, c_2) pair can be recovered by defining the corresponding frame:

$$\begin{cases} c_0 = u^2 v^2 \\ c_2 = -(u^2 + v^2) \end{cases} \Leftrightarrow \begin{cases} u^2 = -\frac{1}{2}\left(c_2 + \sqrt{c_2^2 - 4c_0}\right) \\ v^2 = -\frac{1}{2}\left(c_2 - \sqrt{c_2^2 - 4c_0}\right) \end{cases} \tag{2}$$

With equation (1), a smooth frame field with the property along building edges is learned such that at least one field direction is aligned to the polygon tangent direction. Girard et al. (2021) used PolyVector fields rather than vector fields to align the field to the tangent direction at the polygon corners. The frame field is used to prevent the corners of the polygon from being cut off. The neural network learns the field at every pixel of the image. The learning of (u, v) pair per pixel is challenging due to labelling and sign so, the constant (c_0, c_2) pair is learnt in this method which has no sign or ordering ambiguity.

The original frame field learning method takes *H x W* RGB image *I* as input, and the output is a classification map and a frame field. The classification map is made up of two channels, i.e., building interiors (y_{int}) and the building boundaries (y_{edge}). The frame field consists of four channels corresponding to the two coefficients $c_0, c_2 \in C$. The original method utilizes a deep segmentation model as a backbone. This thesis uses U-net Resnet101 architecture as the backbone with a two-channel output corresponding to object interiors and contours. The training is supervised, which requires input image with labelled ground truth $\hat{y}_{int}$. The edges mask, and interior masks are generated from the polygons on the reference dataset by rasterizing them, which is the pre-processing part of the algorithm. The angle calculated from the segments of the reference data is used for the frame field. The model learns the feature extraction from the input data and, with the help of combined loss functions, constrain these tasks to make them consistent.

The segmentation is improved via multi-task learning with the addition of frame fields aligned to object tangents. The method trains the network for pixel-wise classification of objects followed by additional learning of frame field aligned for the object outlines. The method introduces a frame field that increases segmentation performances, such as yielding sharper corners and vectorization information (Girard et al., 2021). Frame field is added to leverage the polygonization with additional structural information and allow complexity tuning of the corner-aware simplification step for handling non-trivial building topology.

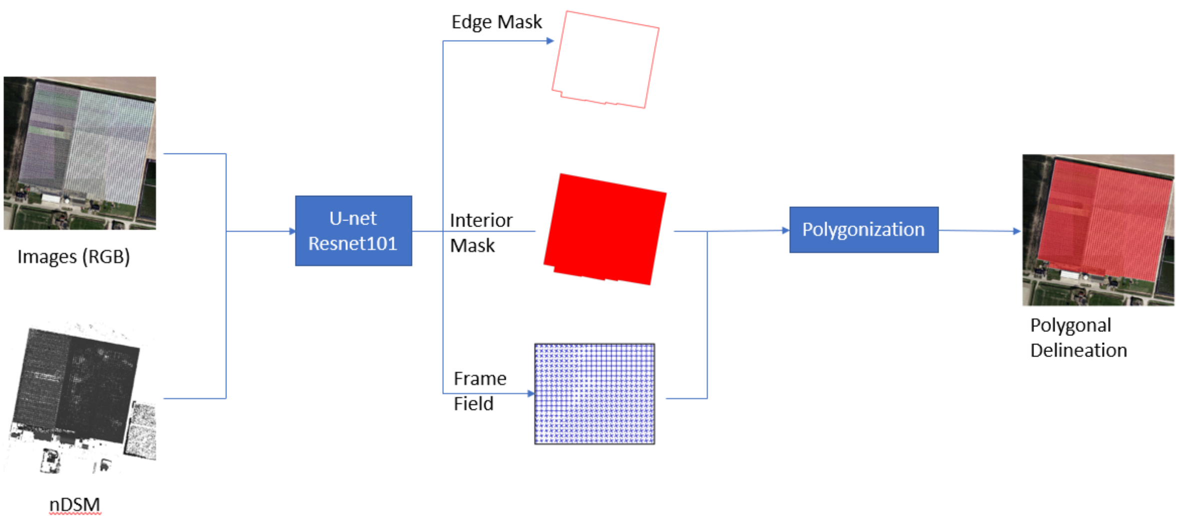

Figure 5: Workflow of investigated frame field learning method for building and adapted for greenhouse delineation by fusing RGB, nDSM data and reference data

Adapted from : (Girard, Smirnov, Solomon, & Tarabalka, 2020)

The input images with the reference data are utilized for segmentation. The base line method frame field learning only utilizes the RGB band, but in this study, nDSM is added to the first layer of the network as the additional layer so that the input images will have four channels. The output features of the backbone are fed to the shallow structures so that the frame field (utilizing four channels) and segmentation (utilizing two channels of the image) are produced.

3.2.1. Loss Function

During the training, there are three different tasks where loss functions were prevalent: a) segmentation, b) frame field and c) coupling losses. The height and width of the input image are denoted by H and W, where linear combined segmentation loss for cross-entropy function and dice function of the edge mask and the interior mask is defined by:

$$L_{BCE}\,(\hat{y}, y) = \frac{1}{HW} \sum_{x \in I} \hat{y}(x).\log\big(y(x)\big) + \big(1 - \hat{y}(x)\big).\log\big(1 - y(x)\big)\,, \tag{3}$$

$$L_{Dice}\,(\hat{y}, y) = 1 - 2\,.\,\frac{|\hat{y}\,.\,y| + 1}{|\hat{y}\; + y| + 1}, \tag{4}$$

$$L_{int} = \alpha\,.\,L_{BCE}\,(\hat{y}_{int}\,, y_{int}) + (1 - \alpha)\,.\,L_{Dice}\,(\hat{y}_{int}\,, y_{int}), \tag{5}$$

$$L_{edge} = \alpha\,.\,L_{BCE}\,\big(\hat{y}_{edge}\,, y_{edge}\big) + (1 - \alpha)\,.\,L_{Dice}\,\big(\hat{y}_{edge}\,, y_{edge}\big), \tag{6}$$

where, L_{BCE} is the binary cross-entropy loss applied and L_{Dice} is the dice loss for the interior mask and the edge mask output of the model. Furthermore, the α is the hyperparameter with the value ranging from 0 and 1.

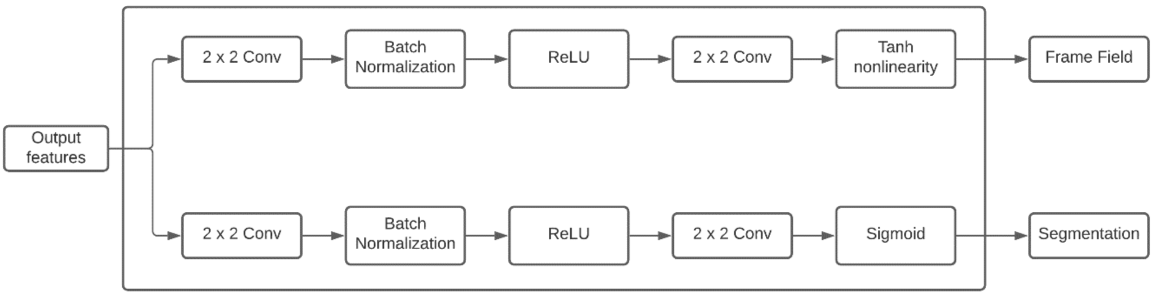

Figure 6: Two branches to produce segmentation and frame field

The frame field is another output from the network obtained through the addition of a fully convolutional network via a module consisting of a sequence of 2 x 2 convolution, batch normalization, an exponential linear unit (ELU) nonlinearity, another 2 x 2 convolution and tanh nonlinearity. The concatenation of the segmentation output and the output feature of the backbone network layer from the frame field. The ground truth label is the angle $\theta_\tau \in [0, \pi)$ of the unsigned tangent vector of the polygon contour. Three losses are considered to train the frame field, which is given by

$$L_{align} = \frac{1}{HW} \sum_{x \in I} \hat{y}_{edge}(x) f(e^{i\theta_\tau}\,;\; c_0(x), c_2(x))^2\,, \tag{7}$$

$$L_{align90} = \frac{1}{HW}\sum_{x\in I} \hat{y}_{edge}(x) f(e^{i\theta_{\tau^{\perp}}}\ ;\ c_0(x), c_2(x))^2\,, \tag{8}$$

$$L_{smooth} = \frac{1}{HW}\sum_{x\in I}\left(\left\|\nabla c_0(x)\right\|^2 + \left\|\nabla c_2(x)\right\|^2\right), \tag{9}$$

The θ_{ω} is the direction of vector $\omega = \left\|\omega\right\|_2 e^{i\theta_{\omega}}$ and $\tau^{\perp} = \tau - \frac{\pi}{2}$. The losses of the different properties of the output field, which is described by L_{align} makes the frame field aligned with the tangent direction of the line segment of the polygon, $L_{align90}$ events the frame field from collapsing into the line field and L_{smooth} is the Dirichlet energy, which measures the smoothness of the function within the location of x in the image.

With different outputs such as interior and boundary segmentation masks, the frame field must be compatible with one another, so coupling losses are added for mutual consistency.

$$L_{int\,align} = \frac{1}{HW}\sum_{x\,\in\,I} f\left(\nabla y_{int}(x);\ c_0(x), c_2(x)\right)^2, \tag{10}$$

$$L_{edge\,align} = \frac{1}{HW}\sum_{x\,\in\,I} f\left(\nabla y_{edge}(x);\ c_0(x), c_2(x)\right)^2, \tag{11}$$

$$L_{int\,edge} = \frac{1}{HW}\sum_{x\,\in\,I} \max(1 - y_{int}(x),\ \|\nabla y_{int}(x)\|_2).\left|\|\nabla y_{int}(x)\|_2 - y_{edge\,(x)}\right| \tag{12}$$

where, $L_{int\,edge}$ aligns the spatial gradient of the predicted interior map y_{int} with the frame field. $L_{edge\,align}$ aligns the spatial gradient of the predicted edge map y_{edge} with the frame field. $L_{int\,edge}$ aligns the interior mask and edge compatible with each other.

The eight losses have different scales and are linearly combined using eight coefficients, so the normalization coefficient $N_{(loss\ name)}$ by averaging each loss on a random subset of the training dataset using a randomly initialized network. The normalization aims to rescale each loss equally, and the combination of main losses and regularization losses are made with parameter $\lambda \in [0,1]$:

$$\lambda\left(\frac{L_{int}}{N_{int}} + \frac{L_{edge}}{N_{edge}} + \frac{L_{align}}{N_{align}}\right) + (1-\lambda)\left(\frac{L_{align90}}{N_{align90}} + \frac{L_{smooth}}{N_{smooth}} + \frac{L_{int\,align}}{N_{int\,align}} + \frac{L_{edge\,align}}{N_{edge\,align}} + \frac{L_{int\,edge}}{N_{int\,edge}}\right) \tag{13}$$

In the original framework, the bias was set with the value $\lambda = 0.75$, and in this thesis, it is also set to 0.50.

3.2.2. Polygonization

For polygonization, interior mask and frame field are the input where the initial contour is extracted from the interior map using the marching squares method (Lorensen & Cline, 1987). Then they are optimized with the active contour method (ACM), which is made to align to the frame field. The corner-aware polygon simplification was utilized by detecting the building corner vertices, one of the important vertices required for delineation.

The polyline collection is polygonised with a list of polygons to detect the building polygons in a planar graph with the building probability value for each polygon with the predicted interior probability map and removing the low-probability polygons.

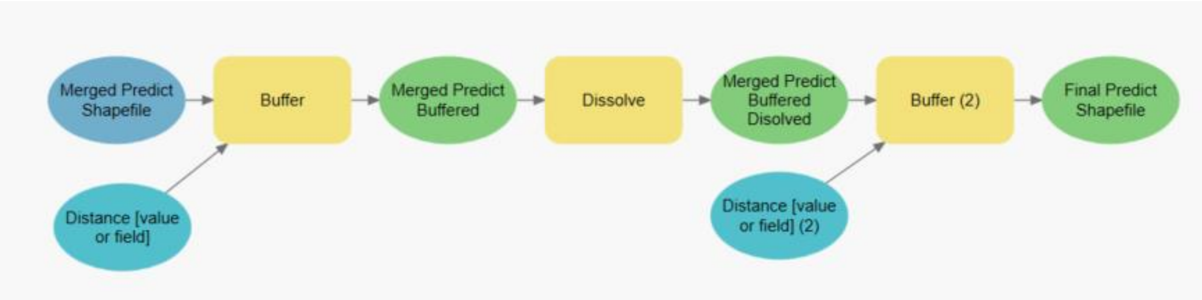

Figure 7: ArcGIS model for aggregating different individual greenhouses separated in the largely dispersed geographical area as shown in figure 9

The output of the predicted test tiles had individual shapefiles per tile. As per the BRT dataset, the size of the greenhouse ranges from 200 sqm to 589653.408 sqm. Since the size of the greenhouses are big and distributed over a large geographical area, a model in ArcGIS was created to aggregate the predicted individual greenhouses in the test dataset. The greenhouses which were separated into two or more tiles, would delineate separately as the model outputs the polygonization per image tiles in the test dataset. For joining such greenhouses together, the ArcGIS model was implemented. The individual predicted shapefiles per image tiles did not overlap with each other and had some gaps, as shown in figure 8-a. While manually checking the distance between the non-overlapped part, it was found to be less than 0.5m for one instance of the greenhouse. So, those individual predicted shapefiles were first merged together in the ArcGIS then was buffered within a distance of 0.5m, as shown in figure 8-b. The resultant was then dissolved such that the overlapped polygon are combined into a single polygon, as shown in figure 8-c. Since buffer was added with the distance of 0.5m, the vector polygon would increase with the distance of 0.5 than the original polygon, so a negative buffer was added. The distance value was set to -0.5m, and the negative buffer was done so that the final joined predicted polygon of the greenhouse was obtained, as shown in figure 8-d. Figure 8-e shows the difference of 0.5m prediction of buffered boundary and negative buffered boundary.

a. Predicted merged individual shapefile *b. Predicted buffered shapefile* *c. Predicted dissolved shapefile*

d. Predicted final shapefile

e. Zoomed layer showing the buffered and negative buffered result

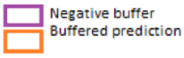

Figure 8: Application example of ArcGIS model on the test dataset

4. MATERIALS

This chapter introduces the study area where the research was conducted, followed by the datasets used. Finally, the description of the data preparation is described.

4.1. Study Area

This research was applied to three different provinces of the Netherlands out of twelve, namely Noord-Holland, Zuid-Holland and Noord-Brabant. Based on the BRT dataset for the greenhouses in the year 2019, there were 13306 greenhouses covering an area of 132829632.50 sq m (132.83 sq km) in the Netherlands. Out of which, 2131 greenhouses covering an area of 1333163.85 sq m (1.33 sq km) were distributed in these three provinces. There were mainly two types of greenhouses present in the area, made up of glasses and plastic. The commercialized greenhouses and movable greenhouses were mainly made up of glasses while, in the farm area (rural part), a few plastic greenhouses were present. Greenhouses had been used for different purposes, such as department stores and greenhouse warehouses for horticulture and vegetation. Greenhouses in the Netherlands are distributed throughout the country, but the study area was selected such that commercialized greenhouses, movable greenhouses, small greenhouses were present. Also, greenhouses near building areas were considered.

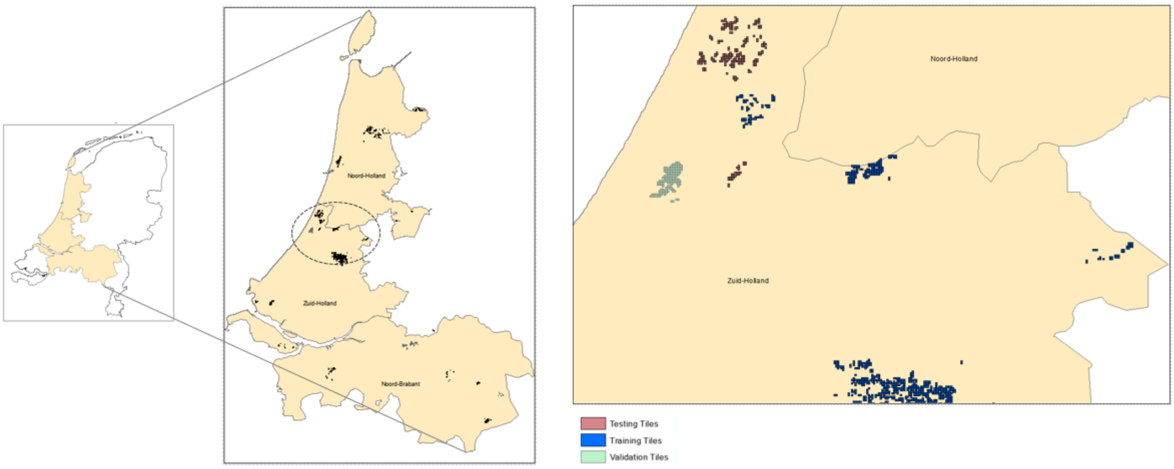

Figure 9: Location of the study area with the distribution of training, testing and validation tiles

4.2. Data

The dataset contains three parts: a) A VHR orthophoto aerial image, b) nDSM generated from stereo imagery, and c) BRT polygon of the greenhouse as reference data.

4.2.1. Aerial Imagery

A nationwide aerial photo of the Netherlands is captured bi-annually during the summer and winter months in different resolutions. The dataset with 0.25 m resolution is freely available to the public. Another dataset is of 0.1 m resolution, used internally. The raw aerial imagery is collected and processed to prepare orthophotos geometrically corrected with uniform scale in the "RD-New" map projection as accepted in the Netherlands. After quality control, the final product is made available to the general public (Kadaster, n.d.-b). Two different orthoimages were utilized for the experimental analysis in this study, which is described below:

4.2.1.1. Winter dataset (0.1m resolution dataset)

The winter dataset is the aerial imagery (orthophotos) with the spatial resolution of 10 cm, which is an internal dataset from Kadaster. The aerial dataset utilized was from 2019 for all the training, validation and testing tiles. The orthophotos were of the size 1024x1024 with the file extension of .png as provided by Kadaster. The .png image file also contains a .wld formatted ESRI World (WLD) file containing control points that describe coordinate information for a raster image, including its pixel size, rotation, and coordinate location (ESRI, 2016).

4.2.1.2. Summer dataset (0.25m resolution dataset)

The summer data is freely available to the users via the Publieke Dienstverlening Op de Kaart (PDOK), which translates to Public Services On the Map website. It contains up-to-date and reliable geo datasets. It contains orthophoto mosaics of the entire country with RGB and Color Infrared (CIR) bands. The CIR band was removed, and only the RGB band was used for experimental analysis. A maximum of 5 years of orthophoto mosaics are available meaning, 2015 – 2019 is available (PDOK, n.d.-a). The summer dataset is the freely available imagery dataset with a resolution of 0.25m from the year 2019.

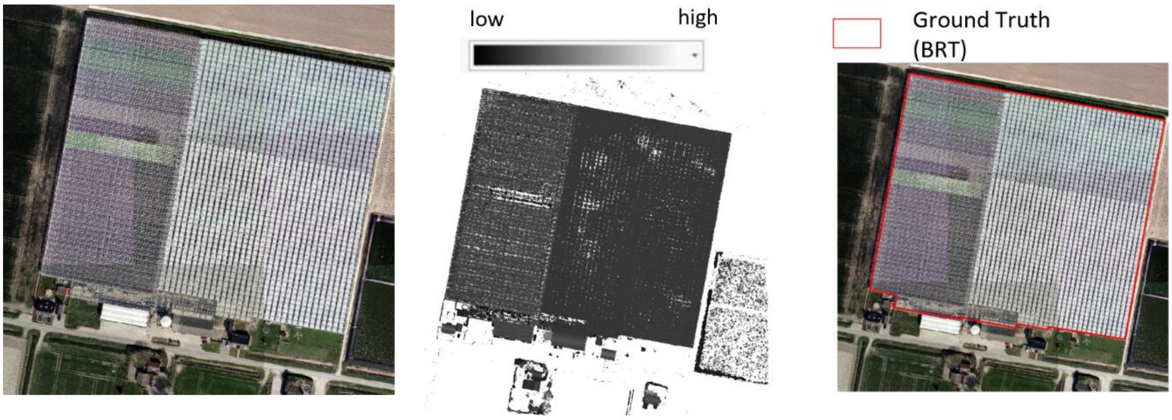

a. Orthophoto (Aerial Image)

b. Normalized Digital Surface Model (nDSM)

c. BRT dataset as the reference data overlapping the aerial image

Figure 10: List of data used

4.2.2. Normalized Digital Surface Model (nDSM)

The nDSM used was also confidential data from Kadaster, which was derived from the VHR stereo imagery. With the overlapped stereo images, the feature points were determined and matched from which 3D coordinates were extracted from the points, which gave the information of 3D information. The nDSM provided was in the form of a raster image with the extension .tif. The nDSM provided the height information of what lies above the ground with a resolution of 0.20m. For winter images, nDSM was resampled into 0.1m.

4.2.3. Greenhouse footprints

The polygonal data was in the ESRI geodatabase format, which can be downloaded from pdok.nl. The greenhouse was one of the attributes within the 'Buildings' category on the TOP10NL product of BRT. Two different categories of the greenhouse were considered "overig|kas,warenhuis" and "kas, wareinhuis", which translated to "other|greenhouse department store" and "greenhouse, warehouse", respectively. There was no separation of plastic greenhouses or glass greenhouses within the attribute of the dataset. The BRT polygons are updated yearly, and the greenhouse footprints of the year 2019 were used for reference purposes.

4.3. Data Preprocessing

The data used in this thesis was VHR resolution images, limiting the research area's size under a certain number of pixels. This is the reason why within the three provinces, not all the greenhouses in the three provinces were selected.

4.3.1. Tiles Preparation, selection and distribution

The training, testing, and validation tiles were distributed over the study area such that geographical knowledge is considered, as mention in section 4.1. Stratified sampling techniques were used within the dataset for training, testing and validation such that there is less class imbalance in terms of greenhouse class and non-greenhouse class. The whole dataset was divided into a sample of a homogeneous dataset with specific criteria. The tiles were distributed for training, validation and testing in which 50% of the tiles were randomly selected, while 50% of the tiles were manually selected. The criteria for selecting the tiles were to have both the glasses greenhouses and the plastic greenhouses. Also, while randomly selecting the tiles, a complete boundary of the greenhouse was not selected due to big sized greenhouses. It means that a part of the greenhouse was being separated as different sets of grouped tiles (validation, training and testing). So, the tiles were manually selected such that a complete polygon lies within a set of grouped tiles. The separation of training, testing and validation tiles were considered with the changes in the greenhouse. The tiles of 1024x1024 were generated using the "Create Fishnet" tools in the ArcGIS for the 0.1m dataset. The tiles were used to clip the images as well as the nDSM.

a. Winter dataset (0.1m resolution)

For 0.1m resolution data, the raster information on the number of columns and the rows was made sure that the rows were 1024x1024 with the cell size to be 0.1. The nDSM was also resampled to 0.1m which was stacked as a 4th channel on top of the RGB images to produce a composite image.

b. Summer dataset (0.25m resolution)

For summer images with the resolution of 0.25m, the tiles generated from the same procedure was of 512x512 such that the cell size was set to 0.25 and the number of columns and rows set to 512x512. The tiles area was considered such that it includes the same area for training, testing and validating areas as compared to the winter dataset. The summer images had some changes in the greenhouses area. Since the time to capture the images was different from the winter dataset, new greenhouses were being built, some greenhouses were being extended, and some greenhouses were demolished.

From the total tiles, 60% of the tiles were selected as training tiles, 20% of tiles as validation and 20% of the tiles as testing datasets. Due to tiles with incomplete polygon among the tiles, the distribution of the tiles was not exactly within the ratio of 60:20:20 for training, testing and validation. The tile distribution, tile size and number of greenhouses within the tiles are shown in the table 4.

Table 4: Information on the tiles used for different datasets, training, validation, and test dataset for experimental analysis

Dataset	Tiles size	Type	Number of Tiles	Number of greenhouses
RGB and RGB+nDSM (0.1m)	1024x1024	training	2303	1760
		validation	422	147
		test	512	224
RGB and RGB (0.25m)	512x512	training	1816	1748
		validation	302	147
		test	398	224

4.3.2. Annotation of the reference dataset

Every individual image tile had its own reference dataset. The name of the tiles of images and the reference data were the same. The reference data, i.e., the polygon of the greenhouse from BRT, was first clipped with respect to the image tiles using the "Clip" tool in ArcGIS. The clipped greenhouse was then split into individual shapefiles using the ArcGIS tool "Split by Attributes". It was used such that the split shapefile would have the same name as the image, with the split field being the name of the image. Two different annotation format was utilized in the thesis which are described below:

a. COCO format

COCO (Common Objects in COntext) format is used mainly in object recognition and scene understanding. The coco format is considered the de facto standard to store the annotations of the object of interest (Waspinator, 2018). It uses .json (JavaScript Object Notation) to encode information about a dataset. It includes the "info", "licenses", "categories", and "images" lists which represents the shapefiles metadata which is written as per the user. The annotations attributes contain information about the bounding box, area, segmentation (shape of the greenhouse), image_id, height and width of the tiles. Figure 11 shows the example of the annotation format for one of the shapefiles and its corresponding image saved in the coco format (Waspinator, 2018).


```
{
    "area": 3030,
    "bbox": [
        984.0,
        510.0,
        40.0,
        149.0
    ],
    "category_id": 1,
    "height": 1024,
    "id": 20,
    "image_id": 20,
    "iscrowd": 0,
    "segmentation": [
        [
            1023.0,
            658.5,
            983.5,
            522.0,
            1021.0,
            509.5,
            1023.5,
            510.0,
            1023.0,
            658.5
        ]
    ],
    "width": 1024
},
```


Figure 11: One of the BRT polygons in COCO dataset JSON format

b. GeoJSON format

The geographic features with the information of the nonspatial format are represented in an open standard geospatial data interchange format termed GeoJSON format (ESRI, n.d.). It is based on the JavaScript Object Notation(JSON) format with information on the type, geographic coordinate reference system, geometry types, and shapefile properties. A snippet of one of the shapefile in the geoJSON file format is shown in figure 12.


```
{
"type": "FeatureCollection",
"crs": { "type": "name", "properties": { "name": "urn:ogc:def:crs:EPSG::28992" } },
"features": [
{
"type": "Feature", "properties": { "Verwerking": "52_22", "PngFileNaa": "2019_hrl_63386_433664_rgb",
"_num_rows": "1024", "_num_colum": "1024", "Verwerki_1": "Zuid-Holland", "Shape_Leng": 409.59999999399997,
"Shape_Area": 10485.7599997 }, "geometry": { "type": "Polygon",
"coordinates": [ [ [ 63487.999999999869033, 433673.79134297312703 ], [ 63485.556999999578693, 433682.87999999942258 ],
[ 63487.999999999869033, 433683.536649409681559 ], [ 63487.999999999869033, 433673.79134297312703 ] ] ] } }
]
}
```


Figure 12: BRT polygon dataset in geoJSON format

4.3.3. Dataset Preparation for the Polymapper

The dataset for the greenhouse was prepared using the aerial image of 0.1m resolution and reference data shapefile of greenhouses from the BRT, shown in figure 13. The shapefile of the reference data was transformed into COCO format to use the method of polymapper, which is shown in figure 10.

a) 0.1m ortho-image b) BRT reference data polygon c) Individual polygon per tiles

Figure 13: Aerial imagery and reference data (BRT polygon) preprocessing

The shapefiles were generated such that the polygon of the object of interest (in this case: greenhouse) was made within the image tiles, meaning that training, validating and testing image tiles and shapefiles with respect to each image tile were equal.

4.3.4. Training the model and reasons for not using Polymapper method for greenhouse

The model was trained with the datasets prepared for the greenhouses. While evaluating the trained model on the test dataset, it did not work. The reason was that the method needs to have at least one complete object of interest per image, i.e., the object of interest (at least one closed polygon per image). Since the greenhouses in the Netherlands are bigger in size with the area of greenhouses which has area up to 500000 sqm., so the initial tiles of 1024 x 1024 was not suitable as a tile did not contain the complete polygon of the greenhouse, but it was divided into different other tiles. The option for bigger image tiles was also not possible because of the cloud machine's memory issues and computational efficiency.

4.3.5. Data Preparation for Frame Field Learning

The dataset tiles were prepared same as mentioned in the section 4.3.1. The dataset for the greenhouse was prepared using the aerial image of 0.1m resolution for winter images, 0.25m resolution for summer image and reference data shapefile of greenhouses from the BRT, shown in figure 13. The shapefile of the reference data per individual tiles was transformed into geoJSON format to use the method of frame field learning method. Furthermore, the mean and the standard deviation of all the training images, testing images and validation images were calculated as it is one of the inputs that need to be set in the model. To train the frame field learning model applicable for greenhouses, two different resolutions of images were taken into account with configuration described in the section 5.1.

5. EXPERIMENTAL ANALYSIS

This chapter describes the experimental analysis done with the information on the configuration, combination of the dataset used, and the evaluation metrics used in the research.

5.1. Configuration

The model was trained with the following settings:

Optimizer:	Adam
Batch size:	1 (Due to CUDA memory error, batch size could not be increased for 0.1m dataset)
Initial learning rate:	0.00001
Exponential decay rate for the learning rate:	0.9
Maximum epoch:	50
Binary cross-entropy:	0.25 (first configuration) and 0.5 (second configuration)
Dice Coefficient:	0.75 (first configuration) and 0.5 (second configuration)
Polygonization parameter:	
Tolerance:	(0.125, 1, 9)

The network is implemented in PyTorch 1.4 and run in a single NVIDIA Tesla P10 GPU setting.

5.2. Combination of the dataset for experimental analysis

Table 5 shows the combination of the datasets for experiment analysis with reference dataset used.

Table 5: Information on the datasets used for the experimental analysis

Experiment Analysis	**Orthoimage of Resolution**	**Bands**	**Reference Dataset**	**Parameter Tuning**
	0.1m (winter data)	RGB	Original Shapefile of BRT	
		RGB	Edited (digitized BRT) shapefile	BCE and Dice coefficient change, tolerance for polygonization
		RGB + nDSM	Edited (digitized BRT) shapefile	BCE and Dice coefficient change, tolerance for polygonization
	0.25m (summer data)	RGB	Edited (digitized BRT) shapefile	BCE and Dice coefficient to be of value 0.25 and 0.75 respectively

5.3. Evaluation Metrics

The quantitative and qualitative result on the experimental analysis in section 5.2. is done based on the combination of the metrics:

5.3.1. Quantitative Analysis

The section describes the metrics that was used during the study.

a) Pixel-level metrics

It represents the per cent of the pixels in the predicted result on the image classified correctly with the reference dataset. In the thesis, Intersection-Over-Union(IoU) is used, which is computed by dividing the area of overlap or intersected area by the area of the union between the predicted segmentation area (p) and the ground truth (g) (Tiu, 2019).

$$IoU = \frac{area\ (p \cap g)}{area\ (p \cup g)}$$

b) Object-level metrics

The delineation of the object of interest is the greenhouse in the thesis, which can be related to object segmentation. For this purpose, mean Average Precision (AP) and mean Average Recall (AR) was calculated with the evaluation metrics used by Common Objects in Context (COCO). The AP and AR have averaged over 10 IoU threshold values of 0.50:0.05:0.95 with 0.05 steps. For better localization, averaging over IoU is calculated (*COCO - Common Objects in Context*, n.d.). AP represents the correctly predicted positive observation ratio to the total predicted positive observation within the IoU threshold. AR represents the ratio of the correctly predicted positive observation to all the predicted observations as the positive class. As per the standard COCO evaluation performance for the object detection, the following metrics are calculated:

Average Precision (AP)	
AP	AP at IoU=0.50:0.05:0.95
$AP^{IoU=.50}$	AP at IoU=0.50
$AP^{IoU=.75}$	AP at IoU=0.75
AP Across Scales	
AP^{small}	AP for small objects: area < 32^2
AP^{medium}	AP for medium objects: 32^2 < area < 96^2
AP^{large}	AP for large objects: area > 96^2
Average Recall (AR)	
$AR^{max=1}$	AR given 1 detection per image
$AR^{max=10}$	AR given 10 detection per image
$AR^{max=100}$	AR given 100 detection per image
AR Across Scales	
AR^{small}	AR for small objects: area < 32^2
AR^{medium}	AR for medium objects: 32^2 < area < 96^2
AR^{large}	AR for large objects: area > 96^2

The standard metrics have evaluation metrics with small objects with an area less than 32^2 pixels, medium objects with an area between 32^2 and 96^2 pixels and large objects with an area greater than 96^2 pixels. AP and AR with the scales of the area are calculated where an area is measured as the number of pixels in the segmentation mask. It was calculated using the standard COCO evaluation for detection metrics by comparing the predicted dataset with the reference dataset.

5.3.2. Qualitative Analysis

Visual inspection or human interpretation was used to check the delineated greenhouse to see if the greenhouse delineations were smooth and free of noise. The test tiles were visually inspected to see whether the predicted boundary of the greenhouse was delineated correctly or not. It was also used to see the false positives of the predicted greenhouses and to see where false positives were common compared to other non-greenhouses classes.

6. RESULT AND DISCUSSION

This chapter includes the quantitative and qualitative analysis of the result obtained from the study. The results are discussed and are followed by the limitation of the research.

The results on the test dataset of the aerial images (RGB) and composite images (RGB+nDSM) within the study area were compared. The model configurations were kept the same to ensure a fair comparison of the experimental analysis while changing the input dataset.

6.1. Quantitative analysis

Table 6 and 7 shows the quantitative results of different experimental analyses done on a different dataset combination as described in section 5.2.

6.1.1. Training on the hyperparameter BCE of 0.25 and Dice Coefficient of 0.75

Table 6: Extracted result on the test dataset on the entire study area with the calculation of mean IoU and standard AP and AR (COCO metrics) for hyperparameter BCE of 0.25 and Dice coefficient of 0.75

Metrics	RGB (0.1m)	RGB+nDSM (0.1m)	RBG (0.25m)
Mean IoU	0.673	0.751	0.745
$AP^{IoU=0.50:0.05:0.95}$	0.005	0.003	0.003
$AP^{IoU=.50}$	0.010	0.007	0.011
$AP^{IoU=.75}$	0.006	0.004	0.006
AP^{small}	0.000	0.000	0.000
AP^{medium}	0.011	0.008	0.010
AP^{large}	0.019	0.017	0.020
$AR^{max=1}$	0.037	0.037	0.038
$AR^{max=10}$	0.056	0.058	0.054
$AR^{max=100}$	0.058	0.058	0.054
AR^{small}	0.000	0.000	0.000
AR^{medium}	0.024	0.017	0.022
AR^{large}	0.063	0.064	0.063

Here, the value of AP^{large} and AR^{small} was 0, which showed that the small greenhouse under the 32^2 pixels and for 0.1 sqm resolution was not visible because the greenhouse was not as small as the greenhouse area bigger than 32^2 x 0.1^2 pixel value. With the threshold of IoU = 0.50, AP of 0.1m RGB images was higher than the RGB + nDSM images indicating that there was the low false positive rate for RGB images, while 0.25 m RGB has the highest among three which indicates that among the three band combination, 0.25 m RGB had low false positive rate. Whereas, RGB + nDSM for 0.1m images had high mean AR value indicating that there were few false negatives. The $AP^{IoU=0.50:0.05:0.95}$ value for 0.1m RGB images was greater than the $AP^{IoU=0.50:0.05:0.95}$ for 0.1m RGB + nDSM with the value of 0.003, meaning within the threshold from 0.5 to 0.95 with the steps of 0.05, the localization was better for 0.10m RGB images.

6.1.2. Training on the hyperparameter BCE of 0.50 and Dice Coefficient of 0.50

Table 7: Extracted result on the test dataset on the entire study area with the calculation of mean IoU and standard AP and AR (COCO metrics) for hyperparameter BCE of 0.50 and Dice coefficient of 0.50

Metrics	RGB (0.1m)	RGB+nDSM (0.1m)
Mean IoU	0.784	0.807
$AP^{IoU=0.50:0.05:0.95}$	0.006	0.004
$AP^{IoU=.50}$	0.011	0.008
$AP^{IoU=.75}$	0.007	0.004
AP^{small}	0.000	0.000
AP^{medium}	0.009	0.009
AP^{large}	0.011	0.015
$AR^{max=1}$	0.049	0.040
$AR^{max=10}$	0.052	0.047
$AR^{max=100}$	0.052	0.047
AR^{small}	0.000	0.000
AR^{medium}	0.020	0.020
AR^{large}	0.058	0.052

With the hyperparameter changed from 0.25 to 0.50 for BCE and 0.75 to 0.75 for Dice coefficient, the mean IoU has increased from 0.673 to 0.784 for 0.10m RGB images and from 0.751 to 0.807 for 0.10m RGB + nDSM images. The $AP^{IoU=0.50:0.05:0.95}$ value for 0.1m RGB images with the value of 0.006 was greater than the $AP^{IoU=0.50:0.05:0.95}$ for 0.1m RGB + nDSM value of 0.004, meaning within the threshold from 0.5 to 0.95 with the steps of 0.05, the localization was better for 0.10m RGB images. With the change of hyperparameter, the accuracy had increased and can be seen in table 7 compared to table 6.

6.2. Qualitative Analysis

The prediction on 0.1m RGB bands after the training the model resulted in following

Reference Dataset Prediction on 0.1m RGB dataset using original BRT shapefile

Figure 14: Prediction on 0.1m RGB dataset using original BRT shapefile done on frame field learning method

Initially, an experiment was conducted with the original datasets from BRT with the frame field learning method. As the area for tiles preparation was selected such that there were changes in terms of greenhouses along with different bigger and smaller greenhouses, the prediction of greenhouses were not good. The greenhouses were being predicted not only in the area where there were greenhouses but also in the vegetation, roads, bare soil areas, and some in the buildings. The reference dataset from BRT was rechecked again and found that there were greenhouses where the image and the reference data polygon were not overlapping with each other, which is seen in figure 15-a. Within the datasets that were prepared for training the datasets initially, it was found that some of the greenhouses were not digitized so the model might have learnt the textural feature and the spectral information of the other classes rather than the greenhouses.

a. Reference data of the greenhouse not overlapping the image.

b. A shift of the greenhouse

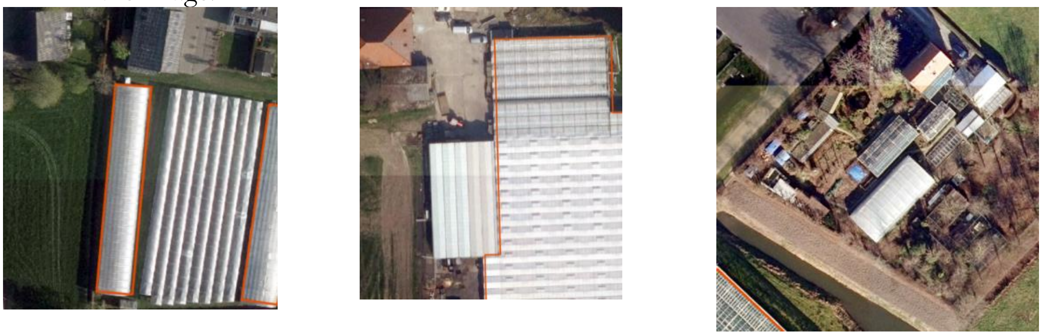

Figure 15: Errors in BRT shapefile within the dataset created

Some of the reference data of the greenhouse were incomplete, meaning only a certain part of the greenhouse had overlapped boundary, while the rest of the greenhouse in the image was not overlapped. Also, some greenhouses have been changed from greenhouse to house and are not updated, resulting in the reference data being something else (e.g. houses) instead of the greenhouse.

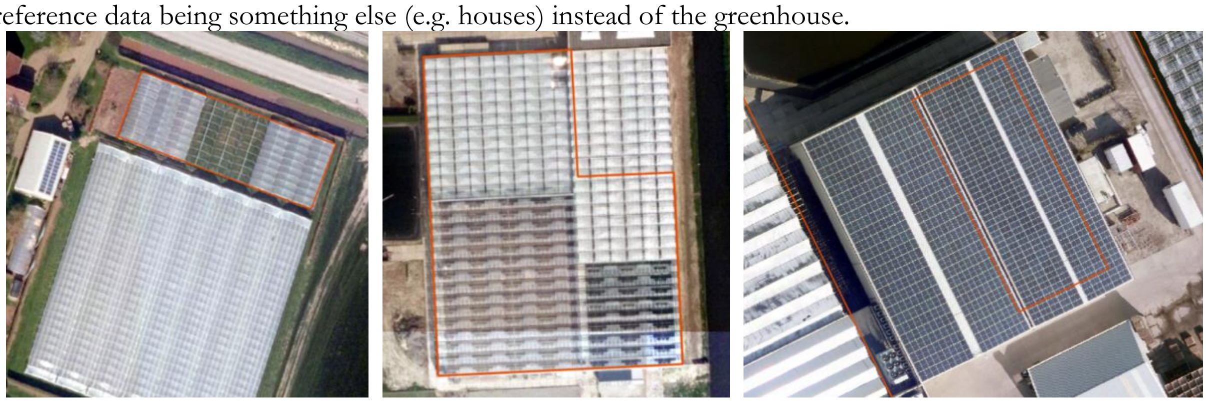

Missing greenhouse reference data

Missing shapefile in the greenhouse (BRT shapefile not properly updated)

Mistake in reference data dataset of greenhouse

Figure 16: Missing BRT polygons and few errors on the BRT polygon shapefile

The dataset was corrected by manually digitizing the polygons which did not match with the orthoimage of 2019. The BRT shapefile where greenhouses were missing, non-overlapped greenhouses, shifted greenhouses were digitized.

The qualitative result obtained in the test set of the aerial images with the dataset combination in section 5.2 with the configuration as mentioned in 5.1 is shown in figure 17 - 19. The red boundary depicts the reference data dataset, blue boundary depicts the predictions on the datasets RGB band with 0.1m, yellow boundary depicts the predictions on the dataset RGB+nDSM band with 0.1m and pink polygon depicts the prediction of the dataset RGB band with 0.25m are shown in the figure 17-18.

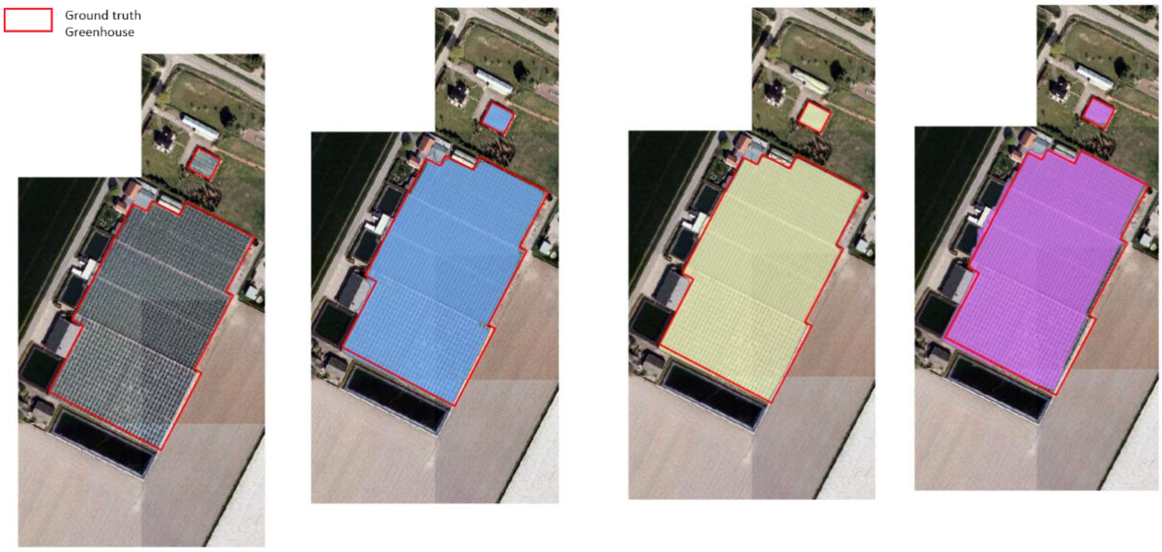

Reference Dataset | Updated or Edited BRT shapefile for 0.1m dataset and 0.25m dataset
Prediction on 0.1m RGB dataset | Prediction on 0.1m RGB+nDSM dataset | Prediction on 0.25m RGB dataset

Figure 17: Prediction of greenhouses with edited BRT shapefiles for a different combination of dataset

The result for prediction of greenhouse has increased vastly compared with the figure 14 and 17 with digitizing the dataset. The prediction on the same area as shown in figure 17 proper delineation of greenhouse, not including prediction on the bare soils or vegetation area.

Reference Dataset | Updated or Edited BRT shapefile for 0.1m dataset and 0.25m dataset
Prediction on 0.1m RGB dataset | Prediction on 0.1m RGB+nDSM dataset | Prediction on 0.25m RGB dataset

In some cases, the 0.1m RGB dataset could not predict greenhouses that were being predicted when nDSM was added to the 0.1m RGB image. It might be due to the elevation data information added to it. Also, 0.25m data was able to predict the greenhouse but could not predict correctly, and polygonization was only in some parts of the greenhouse.

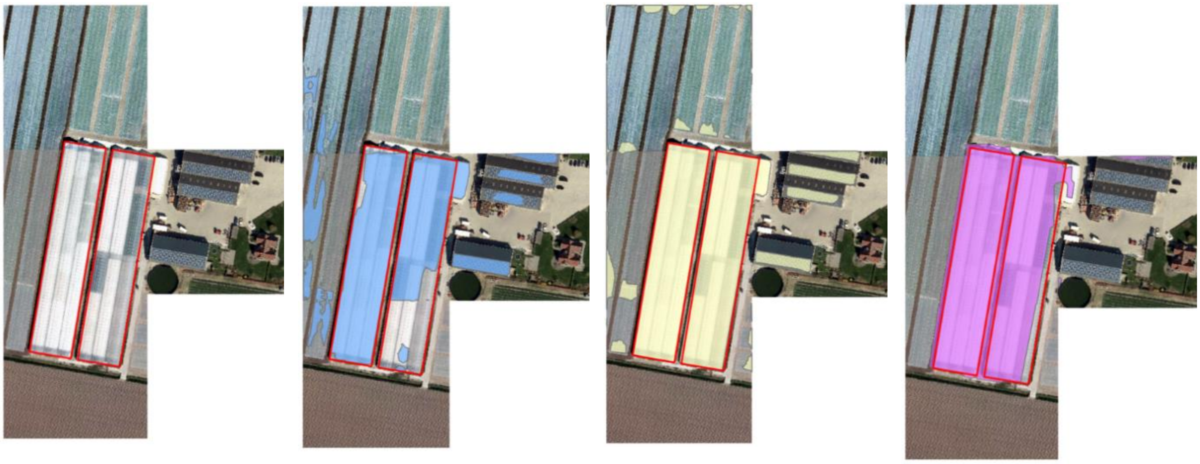

Reference Dataset — Updated or Edited BRT shapefile for 0.1m dataset and 0.25m dataset

Prediction on 0.1m RGB dataset — Prediction on 0.1m RGB+nDSM dataset — Prediction on 0.25m RGB dataset

Figure 18: Prediction of greenhouse in the plastic greenhouse as well as solar panel beside it

The plastic greenhouse is delineated correctly in the 0.1m RGB+nDSM, and in 0.25m RGB data was also able to delineate the greenhouse compared adequately to 0.1m RGB. The figure 18 also shows that the solar panel on the black building is predicted as a greenhouse in both 0.1m RGB+nDSM and 0.1m RGB band.

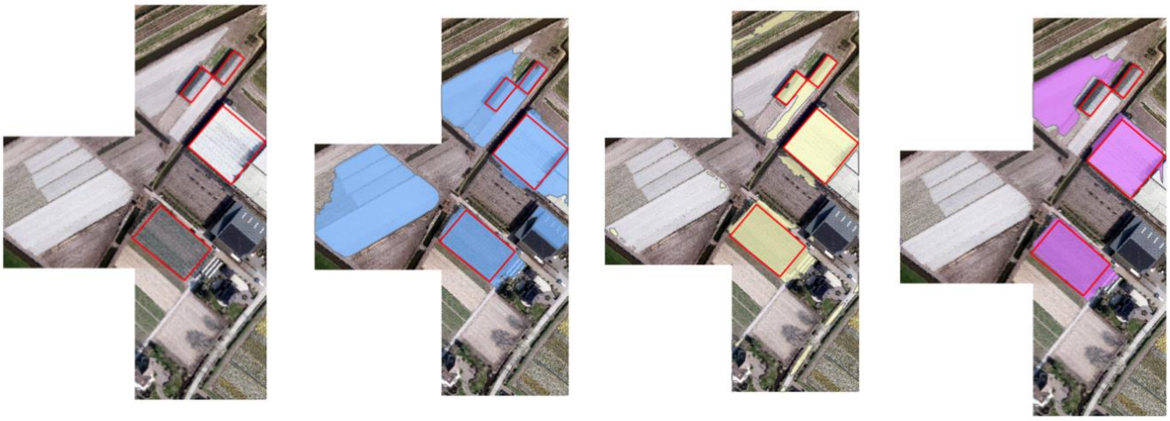

Reference Dataset — Updated or Edited BRT shapefile for 0.1m dataset and 0.25m dataset

Prediction on 0.1m RGB dataset — Prediction on 0.1m RGB+nDSM dataset — Prediction on 0.25m RGB dataset

The RGB 0.1m and 0.25m predicts greenhouses and the bare soils with a similar textural feature as the greenhouse. Adding nDSM has reduced the false positive and predicted the greenhouse, and removed the greenhouse in the ground.

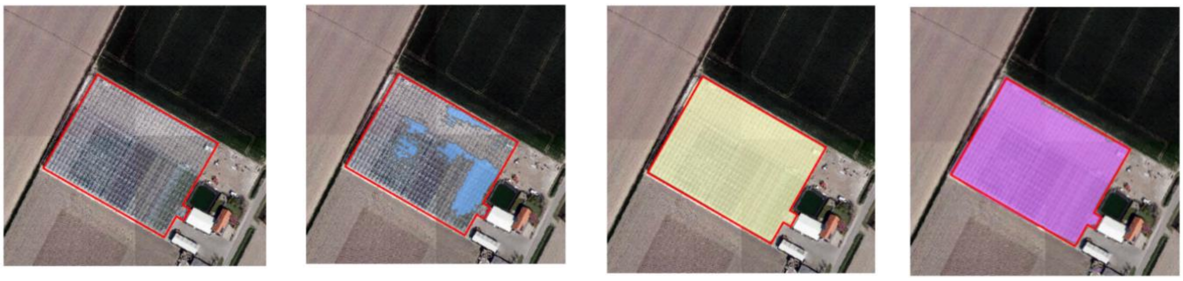

Reference Dataset Updated or Edited BRT shapefile for 0.1m dataset and 0.25m dataset
Prediction on 0.1m RGB dataset Prediction on 0.1m RGB+nDSM dataset Prediction on 0.25m RGB dataset

In some cases, only a small part of the greenhouse was being predicted as a greenhouse in 3band RGB, whereas the addition of nDSM and 0.25m 3RGB had predictions in all the greenhouse areas.

Reference Dataset Updated or Edited BRT shapefile for 0.1m dataset and 0.25m dataset
Prediction on 0.1m RGB dataset Prediction on 0.1m RGB+nDSM dataset Prediction on 0.25m RGB dataset

The buildings with the white roof are being detected as greenhouses relevant in all the experimental analyses.

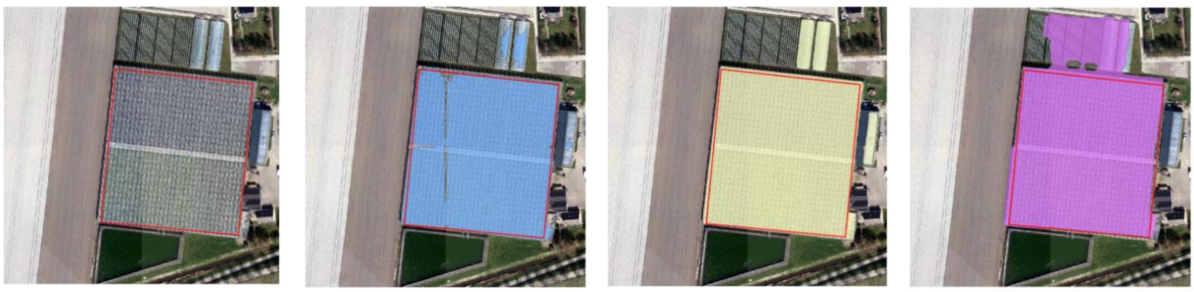

Reference Dataset Updated or Edited BRT shapefile for 0.1m dataset and 0.25m dataset
Prediction on 0.1m RGB dataset Prediction on 0.1m RGB+nDSM dataset Prediction on 0.25m RGB dataset

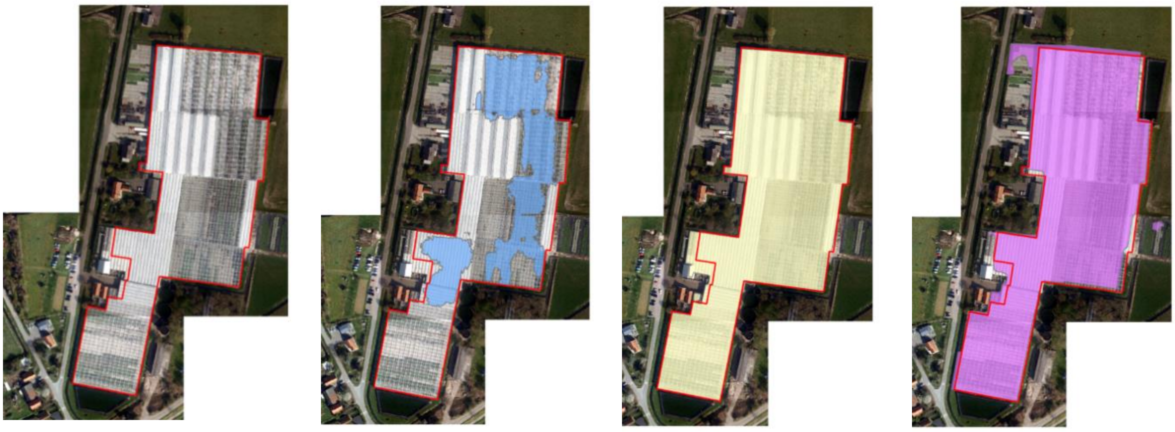

Reference Dataset Updated or Edited BRT shapefile for 0.1m dataset and 0.25m dataset

Prediction on 0.1m RGB dataset Prediction on 0.1m RGB+nDSM dataset Prediction on 0.25m RGB dataset

Reference Dataset Prediction on 0.1m RGB dataset

Prediction on 0.1m RGB+nDSM dataset Prediction on 0.25m RGB dataset

The solar panels are being detected as greenhouses in all the experimental analysis. Kadaster, in one of their work (prediction of solar panel), found that their model was also predicting greenhouse instead of solar panel. In this experiment, we see that for greenhouse prediction, the solar panel was being detected as a greenhouse. It shows that there is some correlation between the greenhouse and the solar panels. There are also solar panels which are part of the greenhouse as one of the ongoing European innovation programs in the southern Netherlands, 'Greenhouse of the Future', which might have resulted in these predictions of greenhouse in the solar panel (*'Greenhouse of the Future' with Special Solar Glass Coming to Netherlands*, 2018).

Reference dataset

Prediction on 0.1m RGB dataset

Prediction on 0.1m RGB+nDSM dataset

Prediction on 0.25m RGB dataset

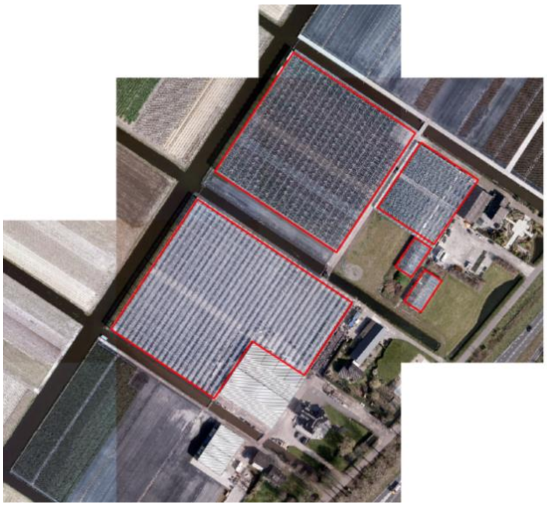

Reference Dataset

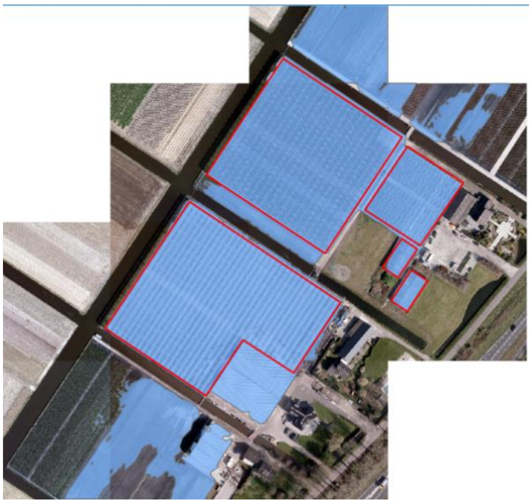

Prediction on 0.1m RGB dataset

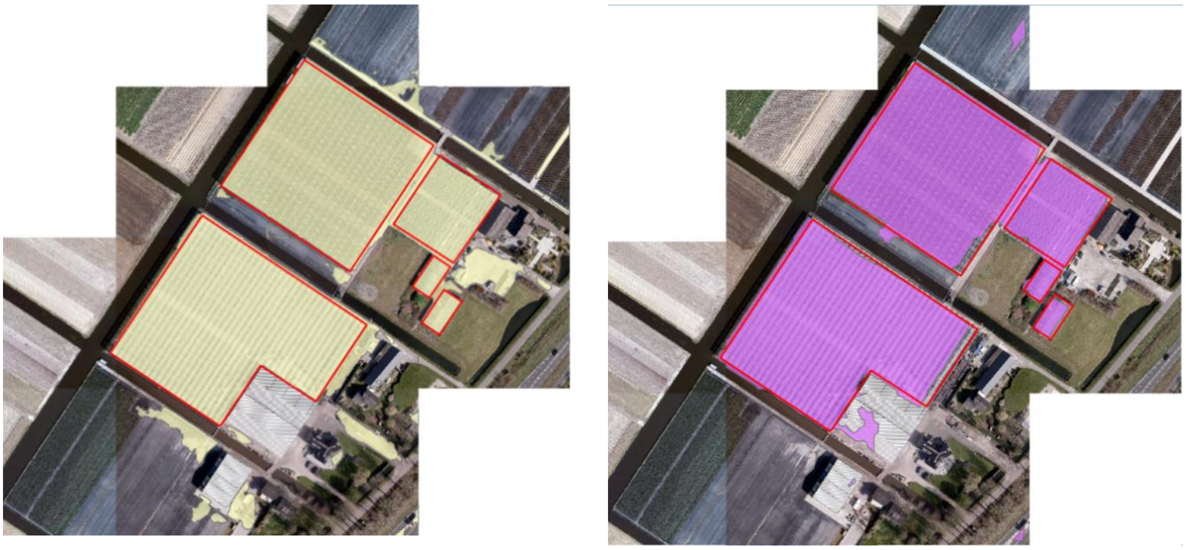

Prediction on 0.1m RGB+nDSM dataset

Prediction on 0.25m RGB dataset

The experimental analysis for the prediction of the polygon of the greenhouse with different tolerance levels (0.125 pixels, 1 pixel and 9 pixels) is shown in figure 19. For polygonization, as the number of tolerance for prediction increases, the number of vertices to make the polygon decreases. While the number of tolerance for prediction decreases, the number of vertices to make the polygon increases.

A predicted polygon with the tolerance of 0.125 pixels for polygonization
Number of vertices = 1468

A predicted polygon with the tolerance of 1 pixel for polygonization
Number of vertices = 674

A predicted polygon with the tolerance of 9 pixels for polygonization
Number of vertices = 395

Figure 19: Example polygon obtained with different tolerance parameters for the polygonization for different band combination

Greenhouses in the Netherlands are mainly made up of glasses, and when aerial images are taken from aircraft, from the position of the sun and the angle of the flights from which greenhouses were taken, there will be a reflection of the glass, resulting in greenhouses with different textures and spectral information. In figure 20, different types of greenhouses in the aerial images are seen: greenhouses are white with a spectral resolution of value 255 all over the greenhouse, transparent greenhouses that reflect clearly what lies underneath. One of the reasons for the detection of the white building as the greenhouse was the training dataset containing white greenhouse, which is the result from the angle from which the image was taken from the aircraft, making the glass of the greenhouse reflects white, as shown in figure 20.

The method was more effective for the greenhouses made up of glasses than greenhouses made up of plastic. The reason can be the fewer plastic greenhouses in general. With the addition of nDSM, the plastic greenhouses were predicted, although there was less training dataset due to additional elevational information.

Figure 20: Greenhouses with different texture

Some greenhouses are transparent, as shown in figure 21, which makes learning during training more difficult, and rather than learning the spectral and textural features of the greenhouse, it learns the underneath information.

Figure 21: Transparent greenhouses

While acquiring the image of the greenhouse, a certain area within the greenhouse reflects the sun and the high-intensity reflection values are obtained in that greenhouse, as shown in figure 22. The spectral and the texture value in that area differs from the, which might have affected the result.

Figure 22: High-intensity reflection in a certain area of the greenhouse while taking an aerial image

6.3. Limitations

The stratification procedure for data preparation might be biased as 50% of the tiles were manually selected with a greenhouse within them. As the greenhouses are big and occupy large areas ranging from 200 sqm to 589653.408 sqm, a complete greenhouse would occupy many tiles. The training, testing and validation tiles were selected such that a complete polygon of the greenhouse lies on one of the three tiles group.

The method of joining the greenhouse that was introduced in section 3.2.2. also has its limitation. The ArcGIS method takes a distance value through which it is buffered. As the method merged and dissolved that predicted polygon together. If the minimal distance between two greenhouses is less than the distance value opted in this method, then the two greenhouses will merge, which will defer the objective of having a single instance of the greenhouse.

The model predicts poor results for plastic greenhouses, which can be seen in figure 18. The distribution of plastic greenhouse in the study area is few. The model is biased towards the plastic and glasses greenhouses due to less number of plastic greenhouses.

7. CONCLUSION AND RECOMMENDATION

This chapter first describes the conclusion of the overall study and later recommends how to improve the methodology further.

7.1. Conclusion

A method used to polygonize the building was utilized for polygonization of the greenhouse, which includes the standard segmentation model with an additional frame field. Adding the nDSM band to the RGB band resulted in incrementing the accuracy and regularity of prediction. For the bigger objects of interest like greenhouses, frame field learning was more appropriate for instance segmentation, as the Polymapper method required to have at least one object of interest with all its boundary within the tiles. The mean IoU for 0.1 m RGB image was 0.673, while for RGB+ nDSM of 0.1 m dataset was 0.751. Some of the greenhouses were not predicted in RGB images of 0.1m resolution, while adding nDSM with the RGB predicted the greenhouse. It concludes that adding nDSM to extract the distinguishes the greenhouses and the background more accurately. The mean IoU of 0.25 m RGB image was 0.745. The results for 0.25m datasets were good in some cases, compared to 0.1m datasets, meaning that only resolution of VHR images cannot only be a factor for better prediction. Greenhouses are big in shape and are visible in both 0.1m and 0.25m datasets. The network can learn spectral and textural features from what is visible from the VHR imagery. The 0.1m RGB images had more distinct texture features that need to be learned, which might have resulted in a poor result than the 0.25m datasets for three RGB bands. For 0.1m datasets, the BCE parameter 0.25 to 0.50 and the Dice coefficient was changed from 0.25 to 0.50, which increases the mean IoU from 0.675 to 0.784 for three-band RGB images and 0.751 to 0.807 for RGB + nDSM images.

The answers to the research questions of the study are presented below:

RQ1: Which deep learning or CNN architecture is appropriate for automated delineation of greenhouses in the polygon format?
Frame field learning method was utilized for the delineation of the greenhouses. The model first produced the classification map by training the deep learning network (UNet-Resnet101) and later vectorised the classified map. Since the greenhouses to be delineated were big, with an area up to 589653.408 sqm, an ArcGIS model was introduced to join the greenhouse together.

RQ2: Which cadastral data sets are suitable for the experimental analysis?
Out of the different key registry in the Netherlands, the BRT dataset contained the footprints of the greenhouse data in the digital format, so the BRT key registry dataset was taken. In terms of images, summer and winter orthoimages were utilized with the resolution of 0.25m and 0.1m, respectively. The summer dataset was freely available which could be downloaded from the open government datasets platform, pdok.nl. The winter orthoimages were private data used for internal uses within the Kadaster. Kadaster took separate flights to produce the winter orthoimages. For the height data, freely available source, i.e., Actueel Hoogtebestand Nederland (AHN) data, was not available for the geographical areas within the year of 2019. So, the nDSM of 2019 with the resolution of 0.2m (which was later resampled for experimental analysis) was used. The nDSM data was internal data of Kadaster that was obtained from the stereophotogrammetry process.

RQ3: Does the normalized Digital Surface Model (nDSM) data contribute to more accurate detection and segmentation of greenhouses?

The quantitative result and the qualitative result shows that the addition of nDSM increases the prediction of greenhouses. The height information contributed to distinguish the greenhouses from the background more accurately, as shown in figure 17 and 18. For BCE coefficient of 0.25 and Dice coefficient of 0.75, the mean IoU of 0.1m RGB images was 0.675, and for 0.1m RGB + nDSM images, the mean IoU value improved to 0.751.

RQ4: What is the effectiveness of the approach for different types of greenhouses (plastics and glasses)?
The study area with greenhouses had a high number of glasses greenhouses compared to plastic greenhouses. The training, validation and testing dataset prepared to apply in the frame field method had more glasses greenhouses, which makes the trained model biased. This is the reason why the prediction of greenhouse shown in figure 18 had a poor prediction for plastic greenhouses. However, the footprint of greenhouses on BRT had no separation of plastic or glasses greenhouse. So, only visual inspection was done to separate the type of greenhouses.

RQ5: Which dataset performs better in terms of delineation of greenhouses?
The height information (nDSM) to the RGB band has increased the prediction of greenhouses compared to the RGB band. The qualitative analysis shows that out of the combination with the same configuration, RGB + nDSM showed better performance with the mean IoU value of 0.751.

RQ6: What is the accuracy of the polygonised greenhouse with the standard metrics?
The accuracy of the predicted greenhouse can be seen in table 6 and 7. The mean IoU value was high for RGB + nDSM dataset with 0.751 for the hyperparameter of 0.25 BCE and 0.75 Dice coefficient. The AP $_{IoU=0.50:0.05:0.95}$ value for 0.1m RGB images was greater than the AP $^{IoU=0.50:0.05:0.95}$ for 0.1m RGB + nDSM with the value of 0.003, meaning within the threshold from 0.5 to 0.95 with the steps of 0.05, the localization was better for 0.10m RGB images. Whereas RGB + nDSM for 0.1m images had a high mean AR value, indicating few false negatives.

RQ7: What are the specification required by Kadaster to update the BRT in terms of the greenhouse?
The specification required by Kadaster to update the BRT is that the greenhouse is considered to be a greenhouse when the digital topographic files, in our case greenhouse, should lie in the scale of at least 1:10000 (Ministerie van Binnenlandse Zaken en Koninkrijksrelaties, n.d.-b). The specification to be a greenhouse was answered by a representative of Kadaster, which is described in section 2.1.3.

RQ8: How can the above technique be used for regular updating of the cadastral database of greenhouses?

To be able to use the current method for a regular update in the cadastral database of the greenhouse, post-processing needs to be done. As the predicted greenhouse has more false positives within buildings with white roofs and solar panels, utilizing the BRT dataset of buildings can help remove the prediction of greenhouses in buildings with white roofs. Since greenhouses do have solar panels above them, they cannot be utilized to remove false positives. Manual professional control is required to verify the correctness of the automatically predicted polygonal greenhouse for updating the cadastral database.

7.2. Recommendation

The proposed methodology can be adopted not only for the objects like a greenhouse but other objects within the digital objects in BRT. Since the original framework, frame field learning was done for building, other objects such as solar panels and storage tanks have been actively being researched in the object detection team within Kadaster. The network can be further improved with the fusing strategy of another layer, such as introducing the nDSM and NIR band for the summer images as an additional layer that might help contribute to more accurate detection and segmentation. As the deep learning method requires a lot of ground truth information to train the model, if the method is going to be applied for the whole of the Netherlands, the training datasets should be significantly increased as only 1.33 sq km of greenhouses are taken into account. Also, the nature of the greenhouse (transparent glasses and some high-intensity values within the greenhouse) can be further reviewed.

The parameters of BCE and Dice coefficient can be further checked in terms of greenhouses; as for buildings, the values of the hyperparameter had good results in 0.25 BCE and 0.75 Dice coefficient value, whereas for the greenhouse, the values with the hyperparameter of 0.50 BCE and 0.50 Dice coefficient has increased the accuracy. Further, using the building information, solar panels information, and road information can be used in post-processing to obtain the greenhouses such that false-positive prediction can be reduced. Furthermore, different polygonization methods or algorithms should be explored, tested, analysed, and compared to calculate the applied method's reliability with other polygonized methods.

LIST OF REFERENCES

Agüera, F., Aguilar, M. A., & Aguilar, F. J. (2006). Detecting greenhouse changes from QuickBird imagery on the Mediterranean coast. *International Journal of Remote Sensing*, *27*(21), 4751–4767. https://doi.org/10.1080/01431160600702681

Agüera, Francisco, Aguilar, F. J., & Aguilar, M. A. (2008a). Using texture analysis to improve per-pixel classification of very high resolution images for mapping plastic greenhouses. *ISPRS Journal of Photogrammetry and Remote Sensing*, *63*(6), 635–646. https://doi.org/10.1016/j.isprsjprs.2008.03.003

Agüera, Francisco, Aguilar, F. J., & Aguilar, M. A. (2008b). Using texture analysis to improve per-pixel classification of very high resolution images for mapping plastic greenhouses. *ISPRS Journal of Photogrammetry and Remote Sensing*, *63*(6), 635–646. https://doi.org/10.1016/j.isprsjprs.2008.03.003

Aguilar, M. A., Saldaña, M. M., & Aguilar, F. J. (2013a). GeoEye-1 and WorldView-2 pan-sharpened imagery for object-based classification in urban environments. *International Journal of Remote Sensing*, *34*(7), 2583–2606. https://doi.org/10.1080/01431161.2012.747018

Aguilar, M. A., Saldaña, M. M., & Aguilar, F. J. (2013b). GeoEye-1 and WorldView-2 pan-sharpened imagery for object-based classification in urban environments. *International Journal of Remote Sensing*, *34*(7), 2583–2606. https://doi.org/10.1080/01431161.2012.747018

Balcik, F. B., Senel, G., & Goksel, C. (2019, July 1). Greenhouse mapping using object based classification and sentinel-2 satellite imagery. *2019 8th International Conference on Agro-Geoinformatics, Agro-Geoinformatics 2019*. https://doi.org/10.1109/Agro-Geoinformatics.2019.8820252

Brownlee, J. (2019). *A Gentle Introduction to Object Recognition With Deep Learning*. Machine Learning Mastery. https://machinelearningmastery.com/object-recognition-with-deep-learning/

Buslaev, A., Seferbekov, S., Iglovikov, V., & Shvets, A. (2018). Fully convolutional network for automatic road extraction from satellite imagery. *IEEE Computer Society Conference on Computer Vision and Pattern Recognition Workshops*, *2018-June*, 207–210. https://doi.org/10.1109/CVPRW.2018.00035

Carrilho, A. C., & Galo, M. (2019). AUTOMATIC OBJECT EXTRACTION FROM HIGH RESOLUTION AERIAL IMAGERY WITH SIMPLE LINEAR ITERATIVE CLUSTERING AND CONVOLUTIONAL NEURAL NETWORKS. *ISPRS - International Archives of the Photogrammetry, Remote Sensing and Spatial Information Sciences*, *XLII-2/W16*(2/W16), 61–66. https://doi.org/10.5194/isprs-archives-XLII-2-W16-61-2019

Carvajal, F., Agüera, F., Aguilar, F. J., & Aguilar, M. A. (2010). Relationship between atmospheric corrections and training-site strategy with respect to accuracy of greenhouse detection process from very high resolution imagery. *International Journal of Remote Sensing*, *31*(11), 2977–2994. https://doi.org/10.1080/01431160902946580

Celik, S., & Koc-San, D. (2019a). Greenhouse Detection from Color Infrared Aerial Image and Digital Surface Model. *Proceedings of 6th International Electronic Conference on Sensors and Applications*, *42*(1), 6548. https://doi.org/10.3390/ecsa-6-06548

Celik, S., & Koc-San, D. (2019b). Greenhouse Detection from Color Infrared Aerial Image and Digital Surface Model. *Proceedings of 6th International Electronic Conference on Sensors and Applications*, *42*(1), 6548. https://doi.org/10.3390/ecsa-6-06548

Celik, S., & Koc-San, D. (2018). Greenhouse detection using aerial orthophoto and digital surface model. *Smart Innovation, Systems and Technologies*, *76*, 51–59. https://doi.org/10.1007/978-3-319-59480-4_6

Chen, K., Pang, J., Wang, J., Xiong, Y., Li, X., Sun, S., Feng, W., Liu, Z., Shi, J., Ouyang, W., Loy, C. C., & Lin, D. (2019). Hybrid Task Cascade for Instance Segmentation. *Proceedings of the IEEE Computer Society Conference on Computer Vision and Pattern Recognition*, *2019-June*, 4969–4978. http://arxiv.org/abs/1901.07518

Cheng, G., Han, J., & Lu, X. (2017). Remote Sensing Image Scene Classification: Benchmark and State of the Art. In *Proceedings of the IEEE* (Vol. 105, Issue 10, pp. 1865–1883). Institute of Electrical and Electronics Engineers Inc. https://doi.org/10.1109/JPROC.2017.2675998

COCO - Common Objects in Context. (n.d.). COCO. Retrieved August 6, 2021, from https://cocodataset.org/#detection-eval

Digitale-overheid.nl. (n.d.). *Key Register Large-Scale Topography (BGT)*. Retrieved September 21, 2020, from https://www.digitaleoverheid.nl/overzicht-van-alle-onderwerpen/basisregistraties-en-stelselafspraken/inhoud-basisregistraties/bgt/

Gandhi, R. (2018). R-CNN , Fast R-CNN , Faster R-CNN , YOLO — Object Detection Algorithms

Understanding object detection algorithms R-CNN. *Medium*, 1–11. https://towardsdatascience.com/r-cnn-fast-r-cnn-faster-r-cnn-yolo-object-detection-algorithms-36d53571365e
Girard, N., Smirnov, D., Solomon, J., & Tarabalka, Y. (2020). *Regularized building segmentation by frame field learning*. IEEE International Geoscience and Remote Sensing Symposium. https://doi.org/10.1109/IGARSS39084.2020.9324080
Girard, N., Smirnov, D., Solomon, J., & Tarabalka, Y. (2021). *Polygonal building extraction by frame field learning*. https://github.com/Lydorn/
Girshick, R., Donahue, J., Darrell, T., & Malik, J. (2014). Rich feature hierarchies for accurate object detection and semantic segmentation. *Proceedings of the IEEE Computer Society Conference on Computer Vision and Pattern Recognition*, 580–587. https://doi.org/10.1109/CVPR.2014.81
González-Yebra, Ó., Aguilar, M. A., Nemmaoui, A., & Aguilar, F. J. (2018). Methodological proposal to assess plastic greenhouses land cover change from the combination of archival aerial orthoimages and Landsat data. *Biosystems Engineering*, *175*, 36–51. https://doi.org/10.1016/j.biosystemseng.2018.08.009
Government.nl. (n.d.). *Municipalities' tasks*. Retrieved October 12, 2020, from https://www.government.nl/topics/municipalities/municipalities-tasks
'Greenhouse of the Future' with special solar glass coming to Netherlands. (2018). Horti Daily. https://www.hortidaily.com/article/6042937/greenhouse-of-the-future-with-special-solar-glass-coming-to-netherlands/
He, K., Gkioxari, G., Dollár, P., & Girshick, R. (2020). Mask R-CNN. *IEEE Transactions on Pattern Analysis and Machine Intelligence*, *42*(2), 386–397. https://doi.org/10.1109/TPAMI.2018.2844175
Hemmati, M. (2002). *Multi-stakeholder Processes for Governance and Sustainability*. Earthscan Publications Ltd.
Hoeser, T., & Kuenzer, C. (2020). Object Detection and Image Segmentation with Deep Learning on Earth Observation Data: A Review-Part I: Evolution and Recent Trends. *Remote Sensing*, *12*(10), 1667. https://doi.org/10.3390/rs12101667
Iglovikov, V., Seferbekov, S., Buslaev, A., & Shvets, A. (2018). TernausNetV2: Fully convolutional network for instance segmentation. *IEEE Computer Society Conference on Computer Vision and Pattern Recognition Workshops*, *2018-June*, 228–232. https://doi.org/10.1109/CVPRW.2018.00042
Information about the Register of Large-scale Topography (BGT) - Land Registry business. (n.d.). Retrieved June 16, 2020, from https://zakelijk.kadaster.nl/bgt
Ji, S., Shen, Y., Lu, M., & Zhang, Y. (2019). Building Instance Change Detection from Large-Scale Aerial Images using Convolutional Neural Networks and Simulated Samples. *Remote Sensing*, *11*(11), 1343. https://doi.org/10.3390/rs11111343
Kadaster. (n.d.-a). *About us - Kadaster*. Retrieved October 12, 2020, from https://www.kadaster.com/about-kadaster
Kadaster. (n.d.-b). *Dataset: Aerial / PDOK (Open)*. PDOK. Retrieved August 20, 2021, from https://www.pdok.nl/introductie/-/article/luchtfoto-pdok
Kadaster. (n.d.-c). *Key Register Large-Scale Topography (BGT)*. Retrieved September 21, 2020, from https://www.kadaster.nl/zakelijk/registraties/basisregistraties/bgt
Kadaster. (n.d.-d). *TOP10NL - Product information - Land Registry business*.
Kadaster. (2020). *Basisregistratie Topografie: Catalogus en Productspecificaties*. https://www.kadaster.nl/documents/1953498/2762084/BRT+catalogus+productspecificaties.pdf/8d315269-a40f-819c-6a58-7e85b59b6718?t=1588864445108
Kaiser, P., Wegner, J. D., Lucchi, A., Jaggi, M., Hofmann, T., & Schindler, K. (2017). Learning Aerial Image Segmentation from Online Maps. *IEEE Transactions on Geoscience and Remote Sensing*, *55*(11), 6054–6068. https://doi.org/10.1109/TGRS.2017.2719738
Key Register Topography (BRT). (n.d.). Retrieved September 23, 2020, from https://www.kadaster.nl/zakelijk/registraties/basisregistraties/brt
Koc-San, D., & Sonmez, N. K. (2016). Plastic and glass greenhouses detection and delineation from Worldview - 2 Satellite Imagery. *ISPRS - International Archives of the Photogrammetry, Remote Sensing and Spatial Information Sciences*, *XLI-B7*, 257–262. https://doi.org/10.5194/isprs-archives-xli-b7-257-2016
Koc-San, Dilek. (2013a). Evaluation of different classification techniques for the detection of glass and plastic greenhouses from WorldView-2 satellite imagery. *Journal of Applied Remote Sensing*, *7*(1), 073553. https://doi.org/10.1117/1.jrs.7.073553
Koc-San, Dilek. (2013b). Evaluation of different classification techniques for the detection of glass and plastic greenhouses from WorldView-2 satellite imagery. *Journal of Applied Remote Sensing*, *7*(1),

073553. https://doi.org/10.1117/1.jrs.7.073553
Krizhevsky, A., Sutskever, I., & Hinton, G. E. (2012). ImageNet Classification with Deep Convolutional Neural Networks. *In Advances in Neural Information Processing Systems*, *25*(Pereira, F., Burges, C.J.C., Bottou, L., Weinberger, K.Q., Eds.; Curran Associates; Red Hook, NY, USA,), 1097–1105. https://papers.nips.cc/paper/4824-imagenet-classification-with-deep-convolutional-neural-networks.pdf
Li, M., Lafarge, F., & Marlet, R. (2020). Approximating shapes in images with low-complexity polygons. *Proceedings of the IEEE Computer Society Conference on Computer Vision and Pattern Recognition*, 8630–8638. https://doi.org/10.1109/CVPR42600.2020.00866
Li, Z., Wegner, J. Di., & Lucchi, A. (2019). Topological map extraction from overhead images. *Proceedings of the IEEE International Conference on Computer Vision*, *2019-October*, 1715–1724. https://doi.org/10.1109/ICCV.2019.00180
Ling, H., Gao, J., Kar, A., Chen, W., & Fidler, S. (2019). Fast Interactive Object Annotation with Curve-GCN. *Proceedings of the IEEE Computer Society Conference on Computer Vision and Pattern Recognition*, *2019-June*, 5252–5261. https://arxiv.org/abs/1903.06874v1
Liu, P. L. (2020). *Single Stage Instance Segmentation — A Review*. Towards Data Science. https://towardsdatascience.com/single-stage-instance-segmentation-a-review-1eeb66e0cc49
Liu, S., Qi, L., Qin, H., Shi, J., & Jia, J. (2018). Path Aggregation Network for Instance Segmentation. *Proceedings of the IEEE Computer Society Conference on Computer Vision and Pattern Recognition*, 8759–8768. https://doi.org/10.1109/CVPR.2018.00913
Long, J., Shelhamer, E., & Darrell, T. (2015). Fully convolutional networks for semantic segmentation. *Proceedings of the IEEE Computer Society Conference on Computer Vision and Pattern Recognition*, *07-12-June-2015*, 3431–3440. https://doi.org/10.1109/CVPR.2015.7298965
Lorensen, W. E., & Cline, H. E. (1987). MARCHING CUBES: A HIGH RESOLUTION 3D SURFACE CONSTRUCTION ALGORITHM. *Proceedings of the 14th Annual Conference on Computer Graphics and Interactive Techniques - SIGGRAPH '87*, *21*(4). https://doi.org/10.1145/37401
Ministerie van Binnenlandse Zaken en Koninkrijksrelaties. (n.d.-a). *Key Register Large-Scale Topography*. Retrieved September 13, 2020, from https://www.geobasisregistraties.nl/basisregistraties/bgt/basisregistratie-grootschalige-topografie
Ministerie van Binnenlandse Zaken en Koninkrijksrelaties. (n.d.-b). *Key Register Topography*. Geo Basic Registrations | The Geobasic Registrations. Retrieved August 9, 2021, from https://www.geobasisregistraties.nl/basisregistraties/topografie
Ministerie Van Binnenlandse Zaken en Koninkrijksrelaties. (n.d.). *The geobasic registrations*. Geo Basic Registrations. Retrieved August 9, 2021, from https://www.geobasisregistraties.nl/basisregistraties
Montoya-Zegarra, J. A., Wegner, J. D., Ladický, L., & Schindler, K. (2015). Semantic Segmentation of Aerial Imges in Urban Areas with class-specific higher order cliques. *ISPRS Annals of Photogrammetry, Remote Sensing and Spatial Information Sciences*, *II-3/W4*(3W4), 127–133. https://doi.org/10.5194/isprsannals-II-3-W4-127-2015
Novelli, A., Aguilar, M. A., Nemmaoui, A., Aguilar, F. J., & Tarantino, E. (2016). Performance evaluation of object based greenhouse detection from Sentinel-2 MSI and Landsat 8 OLI data: A case study from Almería (Spain). *International Journal of Applied Earth Observation and Geoinformation*, *52*, 403–411. https://doi.org/10.1016/j.jag.2016.07.011
Pan, X., Yang, F., Gao, L., Chen, Z., Zhang, B., Fan, H., & Ren, J. (2019). Building extraction from high-resolution aerial imagery using a generative adversarial network with spatial and channel attention mechanisms. *Remote Sensing*, *11*(8). https://doi.org/10.3390/rs11080966
Potlapally, A., Chowdary, P. S. R., Raja Shekhar, S. S., Mishra, N., Madhuri, C. S. V. D., & Prasad, A. V. V. (2019). Instance Segmentation in Remote Sensing Imagery using Deep Convolutional Neural Networks. *Proceedings of the 4th International Conference on Contemporary Computing and Informatics, IC3I 2019*, 117–120. https://doi.org/10.1109/IC3I46837.2019.9055569
Ramer, U. (1972). An iterative procedure for the polygonal approximation of plane curves. *Computer Graphics and Image Processing*, *1*(3), 244–256. https://doi.org/10.1016/S0146-664X(72)80017-0
Saito, S., & Aoki, Y. (2015). Building and road detection from large aerial imagery. In E. Y. Lam & K. S. Niel (Eds.), *Image Processing: Machine Vision Applications VIII* (Vol. 9405, p. 94050K). SPIE. https://doi.org/10.1117/12.2083273
Shi, L., Huang, X., Zhong, T., & Taubenbock, H. (2020). Mapping Plastic Greenhouses Using Spectral Metrics Derived from GaoFen-2 Satellite Data. *IEEE Journal of Selected Topics in Applied Earth Observations and Remote Sensing*, *13*, 49–59. https://doi.org/10.1109/JSTARS.2019.2950466

Shrestha, S., & Vanneschi, L. (2018). Improved Fully Convolutional Network with Conditional Random Fields for Building Extraction. *Remote Sensing*, *10*(7), 1135. https://doi.org/10.3390/rs10071135
Su, H., Wei, S., Yan, M., Wang, C., Shi, J., & Zhang, X. (2019). Object Detection and Instance Segmentation in Remote Sensing Imagery Based on Precise Mask R-CNN. *International Geoscience and Remote Sensing Symposium (IGARSS)*, 1454–1457. https://doi.org/10.1109/IGARSS.2019.8898573
Tarantino, E., & Figorito, B. (2012). Mapping Rural Areas with Widespread Plastic Covered Vineyards Using True Color Aerial Data. *Remote Sensing*, *4*(7), 1913–1928. https://doi.org/10.3390/rs4071913
Tayara, H., & Chong, K. (2018). Object Detection in Very High-Resolution Aerial Images Using One-Stage Densely Connected Feature Pyramid Network. *Sensors*, *18*(10), 3341. https://doi.org/10.3390/s18103341
Tiu, E. (2019). *Metrics to Evaluate your Semantic Segmentation Model*. Towards Data Science. https://towardsdatascience.com/metrics-to-evaluate-your-semantic-segmentation-model-6bcb99639aa2
Tiwari, K. N. (n.d.). *MI&CAD: Lesson 29. Classification of Greenhouse*.
Zhao, K., Kamran, M., & Sohn, G. (2020). BOUNDARY REGULARIZED BUILDING FOOTPRINT EXTRACTION FROM SATELLITE IMAGES USING DEEP NEURAL NETWORKS. *ISPRS Annals of Photogrammetry, Remote Sensing and Spatial Information Sciences*, *V-2–2020*(2), 617–624. https://doi.org/10.5194/isprs-annals-V-2-2020-617-2020
Zhao, W., Ivanov, I., Persello, C., & Stein, A. (2020). BUILDING OUTLINE DELINEATION: FROM VERY HIGH RESOLUTION REMOTE SENSING IMAGERY TO POLYGONS WITH AN IMPROVED END-TO-END LEARNING FRAMEWORK. *ISPRS - International Archives of the Photogrammetry, Remote Sensing and Spatial Information Sciences*, *XLIII-B2-2*, 731–735. https://doi.org/10.5194/isprs-archives-xliii-b2-2020-731-2020
Zhao, W., Persello, C., & Stein, A. (2021). Building outline delineation: From aerial images to polygons with an improved end-to-end learning framework. *ISPRS Journal of Photogrammetry and Remote Sensing*, *175*, 119–131. https://doi.org/10.1016/J.ISPRSJPRS.2021.02.014
Zorzi, S., & Fraundorfer, F. (2020). *Regularization of Building Boundaries in Satellite Images using Adversarial and Regularized Losses*. 5140–5143. https://arxiv.org/abs/2007.11840v1